Mon. Not. R. Astron. Soc. **395,** 1055–1078 (2009) doi:10.1111/j.1365-2966.2009.14599.x

A refined model for spinning dust radiation

Yacine Ali-Haïmoud,[1⋆] Christopher M. Hirata[1⋆] and Clive Dickinson[2⋆]

[1]*California Institute of Technology, Mail Code 130-33, Pasadena, CA 91125, USA*
[2]*Infrared Processing and Analysis Center, California Institute of Technology, M/S 220-6, Pasadena, CA 91125, USA*

Accepted 2009 February 4. Received 2009 February 4; in original form 2008 December 26

ABSTRACT

We present a comprehensive treatment of the spectrum of electric dipole emission from spinning dust grains, updating the commonly used model of Draine & Lazarian. Grain angular velocity distributions are computed using the Fokker–Planck equation; we revisit the drift and diffusion coefficients for the major torques on the grain, including collisions, grain-plasma interactions and infrared emission. We use updated grain optical properties and size distributions. The theoretical formalism is implemented in the companion code, SPDUST, which is publicly available. The effect of some environmental and grain parameters on the emissivity is shown and analysed.

Key words: radiation mechanisms: non-thermal – dust, extinction – radio continuum: ISM.

1 INTRODUCTION

Observational cosmology has entered an area of high precision, exemplified by the most recent temperature results from sensitive cosmic microwave background (CMB) experiments (Dickinson et al. 2004; Readhead et al. 2004; Kuo et al. 2007; Hinshaw et al. 2009). However, foreground separation and removal remains a major challenge for any CMB measurement (e.g. Eriksen et al. 2008; Leach et al. 2008). In addition to the standard Galactic foregrounds, free–free, synchrotron and thermal dust emission, an unknown 'anomalous' dust-correlated emission has been observed over the last decade, in the microwave region of the spectrum. The anomalous emissions was first interpreted as free–free emission from shock-heated gas by Leitch et al. (1997), but Draine & Lazarian (1998a) showed that this would require an extremely high plasma temperature and a corresponding unrealistic energy injection rate. They proposed instead two possible mechanisms to explain the anomalous microwave emission. One of them is the magnetic dipole emission from thermal fluctuations in the magnetization of interstellar dust grains (Draine & Lazarian 1999). The other possible mechanism, on which the present work focuses, is electric dipole radiation from the smallest carbonaceous grains, described in Draine & Lazarian (1998b), hereafter DL98b. The physical principle is quite straightforward: dust grains are presumably asymmetric, and thus will have a non-zero electric dipole moment. These grains will spin due to interaction with the ambient interstellar medium (ISM) and radiation field, and thus radiate electromagnetic waves due to the rotation of their electric dipole moment. To get the electric dipole radiation spectrum, one thus needs three ingredients: the quantity of small grains, then their dipole moment and finally their rotation rates.

Although the observational interest in electric dipole radiation from spinning dust grains has only grown in the last decade, there is a long standing history of theoretical work on the subject. Erickson (1957) was the first to consider the possibility that rotating dust grains could be the source of non-thermal radio noise. Hoyle & Wickramasinghe (1970) showed that this process was dominated by grains with radius $a \lesssim 10^{-6}$ cm and could lead to radio emission around 10 GHz. Ferrara & Dettmar (1994) estimated the spinning dust emissivity for thermally rotating grains. The first to provide a detailed treatment of rotational excitation of small grains were Rouan et al. (1992). They considered the effect of collisions with gas atoms and absorption and emission of radiation. Anderson & Watson (1993) evaluated the effect of collisions with ions and 'plasma drag' (torques due to the electric field of passing ions).

DL98b provided the first comprehensive study of the rotational dynamics of small grains, including all the previous effects. They evaluated, as a function of grain radius and environmental conditions, rotational damping and excitation rates through collisions, 'plasma drag', infrared emission, emission of electric dipole radiation, photoelectric emission and formation of H_2 molecules. The spectra they provided are now widely used in interpreting ISM microwave emission (e.g. Finkbeiner 2004; Watson et al. 2005; Casassus et al. 2006, 2007, 2008; Dickinson et al. 2007, 2009; Dobler et al. 2008) and for CMB foreground analyses (e.g. Banday et al. 2003; Davies et al. 2006; Bonaldi et al. 2007; Hildebrandt et al. 2007; Gold et al. 2009). Given that the DL98b models are now a decade old, and the recent surge in interest in anomalous emission, it is timely to revisit the theory of spinning dust emission, including the approximations made in DL98b. This is the purpose of this paper.

⋆E-mail: yacine@tapir.caltech.edu (YA-H); chirata@tapir.caltech.edu (CMH); cdickins@ipac.caltech.edu (CD)

As in DL98b, we concentrate on the rotation rate of the grains; the size distribution has been reconsidered by other authors, and the grain dipole moment distribution should be regarded as a model parameter since one cannot compute it from first principles. We first review and generalize DL98b rotational excitation and damping rates. We modify the rotational excitation and damping rates by collisions with neutral species, such that it respects detailed balance in the case where the evaporation temperature is equal to the gas temperature. We include the electric dipole potential when evaluating the effect of collisions with ions. Full hyperbolic trajectories and rotating grains are used when computing the effect of plasma drag. We correct the infrared emission damping rate which was underestimated for a given infrared spectrum. Finally, we use these excitation and damping rates to calculate the grain rotational distribution function by solving the Fokker–Planck equation. Updated grain optical properties and size distribution are used throughout this analysis. An Interactive Data Language (IDL) code implementing the formulae in this paper, SPDUST, is available on the web,[1] and will hopefully allow for a more thorough exploration of the parameter space, as well as model fitting to observations.

The paper is organized as follows. In Section 2, we remind the reader of the electric dipole radiation formula and give the resulting expected emissivity. In Section 3, we discuss the size distribution and dipole moments, along with other grain properties. We then turn to the main thrust of this study, which is the computation of the angular velocity distribution function. The theoretical formalism is exposed in Section 4, which presents the Fokker–Planck equation. Sections 5–9 discuss the various rotational damping and excitation processes: collisions with ions and neutral species, plasma drag, infrared emission, photoelectric emission and random H_2 formation. The reader interested primarily in the predicted emission may wish to proceed directly to Section 10, where we present the resulting emissivity and the effect of various parameters and environmental conditions. Our conclusions are given in Section 11. Appendix A exposes the techniques used to numerically evaluate integrals of rapidly oscillating functions involved in the plasma drag calculation. Appendix B presents an alternate, quantum mechanical derivation of the rotational damping rate through infrared emission.

2 ELECTRIC DIPOLE RADIATION

The power radiated by a dust grain spinning with an angular velocity $\boldsymbol{\omega}$, of electric dipole moment $\boldsymbol{\mu}$, with component $\boldsymbol{\mu}_\perp$ perpendicular to $\boldsymbol{\omega}$, is

$$P = \frac{2}{3}\frac{\boldsymbol{\mu}_\perp^2 \boldsymbol{\omega}^4}{c^3}. \tag{1}$$

This power is emitted at the frequency $\nu = \omega/2\pi$.

To get the emissivity of electric dipole radiation per H atom, in erg s^{-1} sr^{-1} (H atom)$^{-1}$, one needs several ingredients:

(i) The grain size distribution function: $n_{\rm H}^{-1}{\rm d}n_{\rm gr}/{\rm d}a$, which gives the number of dust grains per unit size per H atom.

(ii) The electric dipole moments as a function of grain size a: $\mu(a)$.

(iii) The angular velocity distribution function, $f_{\rm a}(\omega)$, which depends upon the grain radius and environmental conditions. It depends on the angular velocity modulus only in a perfectly isotropic environment, with no strong electromagnetic fields forcing the dipole moments to align in some particular direction.

[1] http://www.tapir.caltech.edu/~yacine/spdust/spdust.html

One then readily gets the emissivity of spinning dust grains per H atom:

$$\frac{j_\nu}{n_{\rm H}} = \frac{1}{4\pi}\int_{a_{\rm min}}^{a_{\rm max}} {\rm d}a \frac{1}{n_{\rm H}}\frac{{\rm d}n_{\rm gr}}{{\rm d}a} 4\pi\omega^2 f_{\rm a}(\omega) 2\pi \frac{2}{3}\frac{\mu_{a\perp}^2\omega^4}{c^3}, \tag{2}$$

where $\omega = 2\pi\nu$.

3 DUST GRAINS PROPERTIES

3.1 Grain shapes

The grains are characterized by their volume-equivalent radius a, such that the grain volume is $4\pi a^3/3$. The radius a is in fact a measure of the number of C atoms in the grain, which we assume to be

$$N_{\rm C} = \frac{4\pi a^3 \rho_{\rm C}}{3 m_{\rm C}} \approx 468 a_{-7}^3, \tag{3}$$

where $\rho_{\rm C} = 2.24\,{\rm g\,cm^{-3}}$ is the density of ideal graphite and $a_{-7} \equiv a/(10^{-7}\,{\rm cm})$.

We follow Draine & Li (2001), hereafter DL01, for the number $N_{\rm H}$ of H atoms in the grains (see their equation 8). Following DL98b, we account for the fact that the smallest grains may be sheetlike,[2] as expected for polycyclic aromatic hydrocarbons (PAHs). We assume that this is the case for $a < a_2 = 6$ Å (this corresponds to $N_{\rm C} \approx 100$ carbon atoms, the size of a large PAH). We model them as discs of thickness $d = 3.35$ Å, the interlayer separation in graphite. In many cases, these grains will be rotating primarily around the axis of largest moment of inertia (Purcell 1979), which is perpendicular to the plane of the grain. When computing various rates, we will usually assume a spherical geometry, with a 'surface-equivalent' radius $a_{\rm s}$ or a 'cylindrical excitation-equivalent' radius $a_{\rm cx}$, defined as

$$4\pi a_{\rm s}^2 \equiv \oint {\rm d}S \quad \text{and} \quad 4\pi a_{\rm cx}^4 \equiv \frac{3}{2}\oint \rho^2 {\rm d}S, \tag{4}$$

where $\rho \equiv r\sin\theta$ is the distance to the axis of symmetry and dS is the surface area element.

Although the assumption of cylindrical grains for $a < a_2$ is not critical, it does have an effect on the spectrum, which is shown in Fig. 1.

3.2 Size distribution

Following Weingartner & Draine (2001a), hereafter WD01a, we adopt the following size distribution for carbonaceous dust, for grain radii $a_{\rm min} = 3.5\,{\rm Å} < a < a_{\rm max} = 100\,{\rm Å}$:

$$\frac{1}{n_{\rm H}}\frac{{\rm d}n_{\rm gr}}{{\rm d}a} = D(a) + \frac{C}{a}\left(\frac{a}{a_t}\right)^\alpha F(a;\beta,a_t) \times \begin{cases} 1, & a_{\rm min} < a < a_t \\ {\rm e}^{-[(a-a_t)/a_c]^3}, & a > a_t \end{cases}, \tag{5}$$

where

$$F(a;\beta,a_t) = \begin{cases} 1+\beta a/a_t, & \beta \geq 0 \\ (1-\beta a/a_t)^{-1}, & \beta < 0 \end{cases}. \tag{6}$$

[2] DL98b allow for a possible population of linear grains, although they do not actually use them.

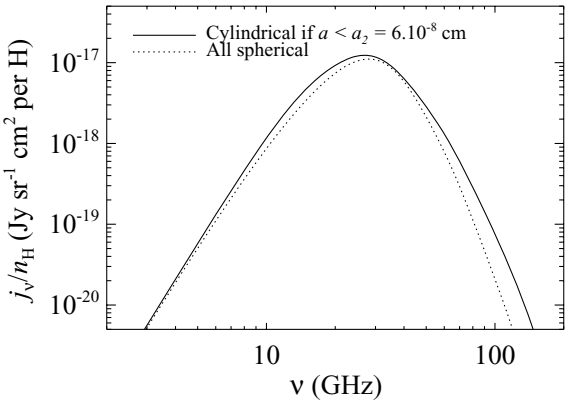

Figure 1. Effect of relaxing the assumption of cylindrical grains on the spectrum, for a fiducial cold neutral medium (CNM) environment (defined in equation 162). At equal radius, spherical grains have a smaller moment of inertia than the cylindrical ones, which are rotating primarily about their axis of largest moment of inertia. They will thus radiate at slightly higher frequencies. For the CNM, we find an increase of peak frequency $\Delta\,\nu_{\rm peak}/\nu_{\rm peak} \approx 6$ per cent. The high-frequency tail of the spectrum is due to the smallest dipole moments of the assumed Gaussian distribution for the intrinsic dipole moments (see Section 3.3 and Fig. 10). For a spherical distribution of dipole moments, there are fewer grains with a low dipole than for a planar distribution. This explains the decrease in power at high frequencies. For the CNM, this results in a decrease of total emitted power $\Delta\, j_{\rm tot}/j_{\rm tot} \approx -16$ per cent.

The function $D(a)$ describes truncated (at 3.5 Å) lognormal grain populations,

$$D(a) = \sum_{i=1}^{2} \frac{B_{\rm i}}{a} \exp\left\{-\frac{1}{2}\left[\frac{\ln(a/a_{0,i})}{\sigma}\right]^2\right\}, \tag{7}$$

with the normalizations $B_{\rm i}$ defined to place a total number $b_{{\rm C},i}$ of carbon atoms per hydrogen nucleus in the ith lognormal population. Here, $b_{\rm C,1} = 0.75 b_{\rm C}$, $b_{\rm C,2} = 0.25 b_{\rm C}$, $b_{\rm C}$ being the total carbon abundance per hydrogen nucleus in the lognormal populations, $a_{0,1} = 3.5$ Å, $a_{0,2} = 30$ Å and $\sigma = 0.4$. This size distribution has a total of six adjustable parameters (b_C, C, a_t, a_c, α, β). For a given choice of b_C, the other five parameters can be found in WD01b, table 1.

We consider only carbonaceous grains in this work. The abundance of small silicate grains in the diffuse phases is indeed limited by the absence of the 10 μm band in emission, as discussed in WD01b. Note, however, that Li & Draine (2001a) found that as much as ∼10 per cent of the interstellar silicate mass could be in the form of ultrasmall particles ($a \lesssim 15$ Å) without violating any existing observational constraints. While consistent with observations, our assumption is thus not required by them.

3.3 Dipole moments

Although only the component of the dipole moment perpendicular to $\boldsymbol{\omega}$ is of importance for the electric dipole emission, the total dipole moment will be needed in coming calculations. In case of spherical grains, we assume the dipole moment and rotation axis are randomly oriented. For cylindrical grains, the dipole moment is mainly oriented in the plane of the grain, perpendicular to the rotation axis.

The dipole moments have two components. First, an intrinsic part $\boldsymbol{\mu}_{\rm i}$, which results from the addition of dipole moments from individual molecular bonds. For a given grain radius, we assume a multivariate Gaussian distribution, with variance proportional to the number of atoms in the grain, $N_{\rm at} = N_{\rm C} + N_{\rm H}$:

$$P(\mu_{\rm i}) \propto \begin{cases} \mu_{\rm i}^2 {\rm e}^{-3\mu_{\rm i}^2/2\langle\mu_{\rm i}^2\rangle} & \text{spherical grains} \\ \mu_{\rm i} {\rm e}^{-\mu_{\rm i}^2/\langle\mu_{\rm i}^2\rangle} & \text{disklike grains} \end{cases}, \tag{8}$$

with

$$\left\langle \mu_{\rm i}^2 \right\rangle = N_{\rm at} \beta^2. \tag{9}$$

These are appropriate assumptions if the dipole moments of bonds add in a random-walk fashion, although we caution that this need not be the case. Counterexamples could include dipole moments dominated by a single feature, e.g. a PAH with a single OH group. The formula given above is in that case intended to give an estimate of the total dipole moment, with the value of β tuned to reproduce approximately observed dipole moments for laboratory molecules (see e.g. DL98b, table 3).

The rms dipole moment per atom, β, is poorly known. Following DL98b, we will take $\beta = 0.38$ debye as a fiducial value, corresponding to

$$\left\langle \mu_{\rm i}^2 \right\rangle |_{a=10^{-7}\,{\rm cm}} = (9.3\,{\rm debye})^2. \tag{10}$$

In addition, for grains with charge Ze, a displacement d between charge centroid and centre of mass (e.g. due to asymmetric grain shape or isotopic substitution) may add another, uncorrelated component. We assume that the displacement is proportional to the excitation equivalent radius: $d = \epsilon a_{\rm cx}$, where $\epsilon = 0.01$ (DL98b). In most cases this is negligible compared to the intrinsic component, so we model it as a single value for the sake of simplicity. The total dipole moment is thus given by

$$\mu^2 = \mu_{\rm i}^2 + (\epsilon Z q_{\rm e} a_{\rm cx})^2, \tag{11}$$

where $q_{\rm e}$ is the elementary charge.

3.4 Grain charge

The rotational damping and excitation rates will be dependent on the grain charge. DL98b showed that the characteristic time-scale for changes in charge is much shorter than the characteristic rotational damping time. We will therefore average the damping and excitation rates over grain charges, as well as the electric dipole moment when computing the power radiated. We therefore need the charge distribution function[3] of the grains as a function of their radius and environmental conditions, $f_{\rm a}(Z)$.

There are three main processes contributing to grain charging: collisional charging by electrons and ions, which rates we denote $J_{\rm e}(Z, a)$ and $J_{\rm i}(Z, a)$, respectively, and photoelectric emission of electrons caused by the impinging radiation, which rate is $J_{\rm pe}(Z, a)$. For every grain radius, the steady state charge distribution function is obtained by solving recursively the following equations:

$$\left[J_{\rm i}(Z,a) + J_{\rm pe}(Z,a)\right] f_{\rm a}(Z) = J_{\rm e}(Z+1,a) f_{\rm a}(Z+1). \tag{12}$$

We use the equations of Draine & Sutin (1987) for collisional processes, updated with the Weingartner & Draine (2001b) electron sticking coefficients for $J_{\rm i}$ and $J_{\rm e}$. The photoelectric emission rate is computed according to WD01b. The radiation field is taken to be a multiple χ of the average interstellar radiation field $u_{\rm ISRF}$, as estimated by Mezger, Mathis & Panagia (1982) and Mathis, Mezger & Panagia (1983).

[3] We use the same notation for different distribution functions. The context and their argument should make their meaning unambiguous.

4 THE FOKKER–PLANCK EQUATION

4.1 Form of the equation in spherical polar coordinates

The stationary angular velocity distribution function $f_{\rm a}(\boldsymbol{\omega})$ [such that $f_{\rm a}(\boldsymbol{\omega})\,{\rm d}^3\boldsymbol{\omega}$ is the probability of the grain's angular velocity being $\boldsymbol{\omega}$ within ${\rm d}^3\boldsymbol{\omega}$] is determined from the stationary Fokker–Planck equation. We differ here from DL98b who assumed the distribution was Maxwellian and calculated its approximate rms grain rotation rate $\langle\omega^2\rangle^{1/2}$. The Fokker–Planck equation is valid in the limit of continuous torques, i.e. if every interaction changing the rotation rate of the grain does so by a small amount $\delta\omega \ll \omega$. This is, therefore, accurate for the largest grains, which have large moments of inertia. But it fails to describe precisely the smallest ones ($a \lesssim 7$ Å), for which DL98b showed that impulsive torques are important (see their section 7 and fig. 7). However, we believe that the actual distribution function would differ from the one we calculate only at very high frequencies, where the dust emissivity is dominated by the vibrational emission. Indeed, the occasional impulsive torques on the grains enhance the distribution function for high values of the rotation rate, where the solution of the Fokker–Planck equation predicts an exponential cut-off, as we shall see later. The peak of the distribution will not be affected significantly, as the variations of the rotation rate of a grain within the peak are not impulsive.

The stationary Fokker–Planck equation is given by

$$\frac{\partial}{\partial\omega^i}\left[D^i(\boldsymbol{\omega})f_{\rm a}(\boldsymbol{\omega})\right] + \frac{1}{2}\frac{\partial^2}{\partial\omega^i\partial\omega^j}\left[E^{ij}(\boldsymbol{\omega})f_{\rm a}(\boldsymbol{\omega})\right] = 0. \tag{13}$$

The coefficients are defined as

$$D^i(\boldsymbol{\omega}) \equiv -\lim_{\delta t\to 0}\frac{\langle\delta\omega^i\rangle}{\delta t} \quad \text{and} \quad E^{ij}(\boldsymbol{\omega}) \equiv \lim_{\delta t\to 0}\frac{\langle\delta\omega^i\delta\omega^j\rangle}{\delta t}. \tag{14}$$

We assume that the medium is isotropic, and there are no physical processes that allow for a preferred direction, such as a magnetic field. As a consequence, the rotational distribution function only depends upon the magnitude ω of $\boldsymbol{\omega}$. Moreover, in a local orthonormal frame $(\hat{\boldsymbol{e}}_\omega, \hat{\boldsymbol{e}}_\theta, \hat{\boldsymbol{e}}_\phi)$, where ω, θ and ϕ are the usual spherical polar coordinates defining $\boldsymbol{\omega}$, the excitation coefficient take up the following form :

$$E^{\hat\omega\hat\omega} = E_\parallel(\omega) \tag{15}$$

accounts for fluctuations along $\hat{\boldsymbol{\omega}}$ and

$$E^{\hat\theta\hat\theta} = E^{\hat\phi\hat\phi} = E_\perp(\omega) \tag{16}$$

accounts for fluctuations perpendicular to $\boldsymbol{\omega}$. The components in the coordinate basis are thus

$$E^{\omega\omega} = E_\parallel(\omega), \quad E^{\theta\theta} = \frac{E_\perp(\omega)}{\omega^2}, \quad E^{\phi\phi} = \frac{E_\perp(\omega)}{\omega^2\sin^2\theta}. \tag{17}$$

Moreover, we assume there are no systematic torques, so the damping coefficient is directed along $\boldsymbol{\omega}$ and we have

$$\boldsymbol{D}(\boldsymbol{\omega}) = D(\omega)\hat{\boldsymbol{e}}_\omega. \tag{18}$$

In the spherical polar coordinate basis, the Fokker–Planck equation then becomes

$$\begin{aligned}&\frac{1}{\omega^2}\frac{\rm d}{{\rm d}\omega}\left[\omega^2 D(\omega)f_{\rm a}(\omega)\right]\\ &+\frac{1}{2\omega^2}\frac{{\rm d}^2}{{\rm d}\omega^2}\left[\omega^2 E_\parallel(\omega)f_{\rm a}(\omega)\right]\\ &-\frac{1}{\omega^2}\frac{\rm d}{{\rm d}\omega}\left[\omega E_\perp(\omega)f_{\rm a}(\omega)\right] \quad = 0.\end{aligned} \tag{19}$$

Integrating once, we get the following first order differential equation:

$$\frac{{\rm d}f_{\rm a}}{{\rm d}\omega} + 2\frac{\tilde D}{E_\parallel}f_{\rm a} = 0, \tag{20}$$

where

$$\tilde D \equiv D + \frac{1}{\omega}(E_\parallel - E_\perp) + \frac{1}{2}\frac{{\rm d}E_\parallel}{{\rm d}\omega}. \tag{21}$$

Note that $\tilde D$ is simply equal to D if the fluctuations are isotropic and independent of ω.

The coefficients D, $E_\parallel$, $E_\perp$, and therefore $\tilde D$ from various independent rotational damping and excitation processes are additive.

A given process is said to respect detailed balance, when, if that process were the only one taking place, the grain would rotate thermally, i.e. $f_{\rm a}(\omega) \propto \exp(-I\omega^2/2kT)$. As one can see from the Fokker–Planck equation, this implies that this process must satisfy

$$\tilde D = \frac{I\omega}{2kT}E_\parallel. \tag{22}$$

Excitation rates are often easier to calculate than damping rates, since they are positively definite and do not rely on near-cancellation of processes that increase or decrease ω. Thus, in some cases, we will make use of detailed balance (i.e. the fluctuation–dissipation theorem), to obtain the damping rate, knowing the excitation rate.

4.2 Normalized damping and excitation coefficients

We will see in the next section that for collisions with neutral H atoms, at a temperature T, for a spherical dust grain at the same temperature T, the damping and parallel excitation coefficients have the following form:

$$\tilde D_{\rm H} = \frac{\omega}{\tau_{\rm H}} \quad \text{and} \quad E_{\parallel,{\rm H}} = E_{\perp,{\rm H}} = \frac{2kT}{I\tau_{\rm H}}, \tag{23}$$

where

$$\tau_{\rm H} \equiv \left[n_{\rm H}m_{\rm H}\left(\frac{2kT}{\pi m_{\rm H}}\right)^{1/2}\frac{4\pi a_{\rm cx}^4}{3I}\right]^{-1} \tag{24}$$

is the characteristic rotational damping time-scale for collisions with neutral H atoms. Note that they respect the detailed balance condition.

We normalize the damping and excitation coefficients of each process to those of collisions with H atoms. Taking DL98b notation, we define, for each process X

$$F_X(\omega) \equiv \frac{\tau_{\rm H}}{\omega}\tilde D_X \tag{25}$$

and

$$G_X(\omega) \equiv \frac{I\tau_{\rm H}}{2kT}E_{\parallel,X}(\omega). \tag{26}$$

A special case is made of the rotational damping through electric dipole radiation (subscript $_{\rm ed}$), because of its specific ω^3 dependence:

$$\left.\frac{\rm d}{{\rm d}t}\left(\frac{1}{2}I\omega^2\right)\right|_{\rm ed} = \frac{2}{3}\frac{\mu_\perp^2\omega^4}{c^3}, \tag{27}$$

so

$$\left.\frac{{\rm d}\omega}{{\rm d}t}\right|_{\rm ed} = -D_{\rm ed}(\omega) = -\frac{2}{3}\frac{\mu_\perp^2\omega^3}{Ic^3} = -\frac{I\omega^3}{3kT}\frac{1}{\tau_{\rm ed}}. \tag{28}$$

Here, we define, following DL98b

$$\tau_{\rm ed} \equiv \frac{I^2c^3}{2kT\mu_\perp^2}. \tag{29}$$

Using equations (25), (26) and (28) in equation (20), the final equation for the distribution function is

$$\frac{{\rm d}f_{\rm a}}{{\rm d}\omega} + \left[\frac{I\omega}{kT}\frac{F}{G} + \frac{\tau_{\rm H}}{\tau_{\rm ed}}\frac{1}{3G}\frac{I^2\omega^3}{(kT)^2}\right]f_{\rm a} = 0, \tag{30}$$

where

$$F \equiv \sum_X F_X \quad \text{and} \quad G \equiv \sum_X G_X. \tag{31}$$

One can see that the conditions to get a thermal, Maxwellian distribution $f_a(\omega) \propto \exp(-I\omega^2/2kT)$ are

$$F = G = \text{constant} \quad \text{and} \quad \frac{\tau_H}{\tau_{ed}} \to 0. \tag{32}$$

Otherwise, the general solution to this equation is

$$f_a(\omega) \propto \exp\left\{ -\int_0^\omega d\omega' \left[\frac{I\omega'}{kT} \frac{F(\omega')}{G(\omega')} + \frac{\tau_H}{3\tau_{ed} G(\omega')} \frac{I^2\omega'^3}{(kT)^2} \right] \right\}. \tag{33}$$

If all F_Xs and G_Xs are constant, this has a simple form

$$f_a(\omega) \propto \exp\left[-\frac{F}{G}\frac{I\omega^2}{2kT} - \frac{\tau_H}{\tau_{ed}} \frac{1}{3G} \left(\frac{I\omega^2}{2kT} \right)^2 \right]. \tag{34}$$

Note that the damping through electric dipole radiation causes the distribution to be non-Maxwellian.

In the general case, some F_Xs and G_Xs may depend upon ω and one has to compute numerically the resulting distribution function using equation (33).

We now turn to the calculation of the various damping and excitation coefficients, due to collisions, plasma drag, infrared emission, photoelectron emission and random H_2 formation. In the following microphysics sections that form the heart of the paper, we compute excitation and damping coefficients as a function of grain radius and environmental conditions. We evaluate them numerically for a fiducial cold neutral medium (CNM) environment, defined explicitly in equation (162).

5 COLLISIONAL DAMPING AND EXCITATION

In this section, we correct the results of DL98b, Appendix B, which did not take into account the fact that not all neutrals escape the grain surface when computing the damping rate. The microphysics of collisions is complex and beyond the scope of this study (for a discussion of the physics and chemistry of PAHs and their relation with the interstellar gas see e.g. Omont 1986). We therefore use the following simplifying assumptions.

(i) The grain is in a stationary state: the rate at which species collide with it is equal to the rate at which they leave its surface.

(ii) We assume that all species (neutrals and ions) colliding with the grain stick and that they depart the grain as neutrals. In extremely dense environments, the colliding species may bounce off the grain surface instead of sticking. This case is discussed at the end of Section 5.1.4.

(iii) Even if the impacting species may not collide equiprobably everywhere on the grain's surface (e.g. if the grain is non-spherical or if it has a dipole moment), we assume they somehow get redistributed on the grain surface and leave it equiprobably from any point.

(iv) We assume, as in DL98b, that neutrals leave the grain surface with a thermal velocity distribution in the grain's frame, with a temperature T_{ev} of the order of the infrared emission characteristic temperature. Unlike DL98b, we estimate T_{ev} as a function of grain radius and ambient radiation field (see Section 5.1.4).

Using those assumptions, one can compute the rate of collisional damping and excitation. We will perform the calculations for a spherical grain in the general case. To find the relevant equivalent radius to use for a cylindrical grain, we will carry out the explicit calculation in the case of collisions of a neutral grain with neutral H atoms. Note that as pointed in DL98b, the rotational excitation in case of collisions has two origins: the random excitation by incoming particles (superscript $^{(in)}$), as well as the random excitation by 'evaporating' neutrals (superscript $^{(ev)}$).

5.1 General considerations: spherical grain

We use the usual spherical polar coordinates around the spherical grain, taking the rotation axis as a reference. The local phase-space density at the grain surface is

$$f_{ev}(\boldsymbol{v}, \theta) = K(\theta) \exp\left[-\frac{m(\boldsymbol{v} - \boldsymbol{v}_0)^2}{2kT_{ev}} \right] \tag{35}$$

with the local velocity

$$\boldsymbol{v}_0 \equiv \boldsymbol{\omega} \times \boldsymbol{r} = a\omega \sin\theta \hat{\boldsymbol{e}}_\phi. \tag{36}$$

The normalization constant $K(\theta)$ is found by imposing that, locally, the flux of evaporating (and escaping) particles is equal to the flux of colliding particles. Except for the case of ions interacting with the electric dipole of the grain, the flux of colliding particles will be homogenous on the grain surface. If it is not the case, we approximate the local flux by the total rate of collisions dN_{coll}/dt divided by the grain area:

$$\frac{1}{4\pi a^2} \frac{dN_{coll}}{dt} = K \int v_r \exp\left[-\frac{m(\boldsymbol{v} - \boldsymbol{v}_0)^2}{2kT_{ev}} \right] P_{esc}\, d^3\boldsymbol{v}, \tag{37}$$

where $P_{esc} = 1$ for velocities at the grain surface leading to escape, and 0 otherwise.

All particles evaporating from the grain are neutrals. They interact with the grain through the induced dipole potential (we neglect the dipole-induced dipole interaction with the dipole moment of the grain):

$$U(r) = -\frac{1}{2}\alpha \frac{Z_g^2 q_e^2}{r^4}, \tag{38}$$

where α is the polarizability of the escaping neutral and q_e is the elementary charge. The polarizability of hydrogen is a standard result in non-relativistic quantum mechanics and is $\frac{9}{2}a_0^3 = 0.67\,\text{Å}^3$ where a_0 is the Bohr radius (Landau & Lifshitz 1965). We also take $\alpha = 0.20\,\text{Å}^3$ for helium[4] (Thomas & Humbertson 1972), and $\alpha = 1.54\,\text{Å}^3$ for carbon (Miller & Kelly 1972), which is important since C^+ is often the dominant ion if the hydrogen is self-shielded. For molecular hydrogen H_2, we take $\alpha = 0.79\,\text{Å}^3$ (Marlow 1965).

5.1.1 *Computation of P_{esc}*

The radial coordinate of the escaping neutral is the solution of the following equation:

$$\dot{r}^2 + V_{eff}(r) \equiv \dot{r}^2 + \frac{a^2}{r^2} v_\parallel^2 - \frac{a^4}{r^4} v_a^2 = \frac{2E}{m}, \tag{39}$$

where $v_\parallel$ is the modulus of the tangential velocity at the grain surface and

$$v_a^2 \equiv \frac{Z_g^2 q_e^2 \alpha}{m a^4}. \tag{40}$$

[4] We assume that all the helium is neutral and $n_{He}/n_H = 1/12$.

The effective potential has a maximum at the radius

$$r_{\rm a} = \sqrt{2}a\frac{v_{\rm a}}{v_\parallel}; \quad V_{\rm eff}(r_{\rm a}) = \frac{v_\parallel^4}{4v_{\rm a}^2}. \tag{41}$$

To escape, a neutral needs to have either $a > r_{\rm a}$ or $2\,E/m > V_{\rm eff}(r_{\rm a})$. These two conditions can be combined to get

$$P_{\rm esc} = 1 \text{ if } \begin{cases} v_{\rm r} > v_{\rm a} & \text{or} \\ 0 < v_{\rm r} < v_{\rm a} & \text{and} \quad v_\parallel > \sqrt{2v_{\rm a}(v_{\rm a} - v_{\rm r})} \end{cases}, \tag{42}$$

where $v_{\rm r}$ is the radial velocity at the grain surface.

5.1.2 Computation of $K(\theta)$

Following DL98b, we define $\epsilon_{\rm e}^2 \equiv mv_{\rm a}^2/2kT_{\rm ev}$, which describes whether the typical evaporating atom has enough energy to overcome the induced dipole attraction to the grain ($\epsilon_{\rm e} < 1$) or not ($\epsilon_{\rm e} > 1$). We also define the ratio of rotational velocity to thermal velocity at the grain surface, which is small compared to unity:

$$\Omega \equiv a\omega\sqrt{\frac{m}{2kT_{\rm ev}}} \sim \left(\frac{m}{m_{\rm grain}}\frac{T_{\rm rot}}{T_{\rm ev}}\right)^{1/2} \ll 1. \tag{43}$$

In terms of those dimensionless quantities, we can find the normalization constant K. The right-hand side of equation (37) can be expanded using the substitution

$$(v_{\rm r}, v_\theta, v_\phi) = \sqrt{\frac{2kT_{\rm ev}}{m}}\,(u_{\rm r}, u\cos\psi, u\sin\psi) \tag{44}$$

to yield

$$\begin{aligned}\frac{1}{4\pi a^2}\frac{{\rm d}N_{\rm coll}}{{\rm d}t} = K\left(\frac{2kT_{\rm ev}}{m}\right)^2\frac{\pi}{2}\Bigg[&{\rm e}^{-\epsilon_{\rm e}^2} \\ &+{\rm e}^{-(\Omega\sin\theta)^2}\int_0^{\epsilon_{\rm e}} 2u_{\rm r}{\rm d}u_{\rm r}\,{\rm e}^{-u_{\rm r}^2} \\ &\times\int_{\sqrt{2\epsilon_{\rm e}(\epsilon_{\rm e}-u_{\rm r})}}^{\infty} 2u\,{\rm d}u\,{\rm e}^{-u^2} I_0(2u\Omega\sin\theta)\Bigg],\end{aligned} \tag{45}$$

where

$$I_0(X) = \frac{1}{2\pi}\int_0^{2\pi}{\rm e}^{X\sin\psi}{\rm d}\psi = 1 + \frac{1}{4}X^2 + \cdots \tag{46}$$

is a modified Bessel function of the first kind.

Expanding to second order in Ω, we get

$$K = \left(\frac{2kT_{\rm ev}}{m}\right)^{-2}\frac{2}{\pi}\frac{{\rm e}^{\epsilon_{\rm e}^2}}{{\rm e}^{-\epsilon_{\rm e}^2} + \sqrt{\pi}\epsilon_{\rm e}\,{\rm erf}\,(\epsilon_{\rm e})}\frac{1}{4\pi a^2}\frac{{\rm d}N_{\rm coll}}{{\rm d}t} \tag{47}$$

up to corrections of order $\mathcal{O}(\Omega^2)$.

5.1.3 Damping and excitation rates

Each escaping neutral particle takes away an angular momentum

$$\boldsymbol{L} = ma(v_\theta\hat{\boldsymbol{e}}_\phi - v_\phi\hat{\boldsymbol{e}}_\theta). \tag{48}$$

As $P_{\rm esc}$ is an even function of v_θ, the average of v_θ vanishes. The loss of angular momentum along the z-direction per unit time per unit area is given by

$$\begin{aligned}\frac{{\rm d}L_{\rm z}}{{\rm d}t\,{\rm d}S} = &-ma\sin\theta K\int v_{\rm r}v_\phi\exp\left[-\frac{m(\boldsymbol{v}-\boldsymbol{v}_0)^2}{2kT_{\rm ev}}\right] \\ &\times P_{\rm esc}\,{\rm d}v_{\rm r}\,{\rm d}v_\theta\,{\rm d}v_\phi.\end{aligned} \tag{49}$$

Here, we differ from DL98b as we take into account the fact that not all particles escape from the grain. Expanding in Ω and using the expression for K we get, up to corrections of order $\mathcal{O}(\Omega^2)$,

$$\frac{{\rm d}L_{\rm z}}{{\rm d}t\,{\rm d}S} = -\frac{1}{4\pi}m\sin^2\theta\,\frac{{\rm e}^{-\epsilon_{\rm e}^2} + 2\epsilon_{\rm e}^2}{{\rm e}^{-\epsilon_{\rm e}^2} + \sqrt{\pi}\epsilon_{\rm e}\,{\rm erf}\,\epsilon_{\rm e}}\frac{{\rm d}N_{\rm coll}}{{\rm d}t}\omega. \tag{50}$$

Integrating over the whole grain surface, we find the damping rate

$$D(\omega) = -\frac{1}{I}\frac{{\rm d}L_{\rm z}}{{\rm d}t} = \frac{{\rm e}^{-\epsilon_{\rm e}^2} + 2\epsilon_{\rm e}^2}{{\rm e}^{-\epsilon_{\rm e}^2} + \sqrt{\pi}\epsilon_{\rm e}\,{\rm erf}\,\epsilon_{\rm e}}\frac{2ma^2}{3I}\frac{{\rm d}N_{\rm coll}}{{\rm d}t}\omega. \tag{51}$$

A similar calculation leads to the excitation rate through evaporating particles:

$$\begin{aligned}E_\parallel^{\rm (ev)}(\omega) &= \frac{1}{I^2}\frac{{\rm d}\Delta L_{\rm z}^{2\,\rm (ev)}}{{\rm d}t} \\ &= \frac{{\rm e}^{-\epsilon_{\rm e}^2} + 2\epsilon_{\rm e}^2}{{\rm e}^{-\epsilon_{\rm e}^2} + \sqrt{\pi}\epsilon_{\rm e}\,{\rm erf}\,\epsilon_{\rm e}}\frac{2ma^2}{3I^2}\frac{{\rm d}N_{\rm coll}}{{\rm d}t}kT_{\rm ev} \\ &= \frac{kT_{\rm ev}}{I\omega}D(\omega),\end{aligned} \tag{52}$$

up to terms quadratic in Ω.

This implies the remarkable relation

$$G_{\rm coll}^{\rm (ev)} = \frac{T_{\rm ev}}{2T}F_{\rm coll}. \tag{53}$$

Physically, this occurs because if $T_{\rm ev} = T$, then the collisions with neutrals satisfy detailed balance, equation (22). The factor of 2 arises since in this case there is an equal contribution to the excitation from incoming and evaporating particles.

We derive a stronger damping rate due to evaporating atoms than DL98b: for $\epsilon_{\rm e} \ll 1$ this results in no change, but for $\epsilon_{\rm e} \gg 1$ we find much stronger damping. The physical origin of this is that atoms that evaporate with prograde velocities relative to the local grain surface ($v_\phi > v_{0\phi}$) typically have more angular momentum than atoms that evaporate with retrograde velocities. Therefore, the centrifugal potential helps them to escape the grain. DL98b neglected this effect, but for $\epsilon_{\rm e} \gg 1$ it is dominant.

The excitation rate through incoming particles will be calculated for each case.

5.1.4 Evaporation temperature $T_{\rm ev}$

DL98b assume that the evaporating temperature is a constant, independent of grain size. This accurately describes the largest grains, for which the temperature may be approximated as a constant, obtained from equating the absorbed and emitted energy (DL98b):

$$T_c = \frac{hc}{k}\left[\frac{\langle Q\rangle_* u_*}{8\pi hcQ_0\lambda_0^\alpha\Gamma(\alpha+4)\zeta(\alpha+4)}\right]^{1/(\alpha+4)}, \tag{54}$$

where in the infrared the grain absorption efficiency is assumed to be a power law

$$Q_\nu = Q_0\left(\frac{\nu}{\nu_0}\right)^\alpha, \quad \lambda_0 = \frac{c}{\nu_0} \tag{55}$$

with typically $\alpha = 2$ and $\langle Q\rangle_* u_* \equiv \int {\rm d}\nu\, Q_\nu u_\nu$. Note that we have $T_c \propto \chi^{1/6}$ and a weak dependence on grain radius as the absorption efficiencies cancel out.

However, the smallest grains undergo sudden thermal spikes after each photon absorption, followed by long intervals during which the grain drops to its vibrational ground state. The neutrals or ions that have stuck to the grain after a collision cannot be thermally ejected from a grain in the ground state so we assume ejection

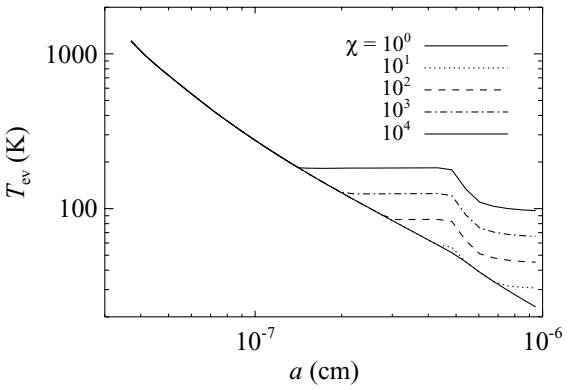

Figure 2. Evaporation temperature T_{ev} as a function of grain radius a, for various values of the ambient radiation field u, parametrized by $\chi = u/u_{ISRF}$. The curves join at small radii, for which the grains undergo temperature spikes. The kink at $a = 50$ Å results from the DL01 prescription for PAH-graphite optical properties.

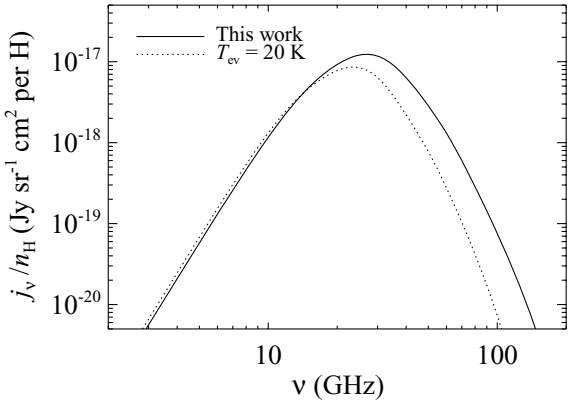

Figure 3. Effect of the evaporation temperature model on the spinning dust spectrum for the cold neutral medium (CNM, equation 162). Our prescription results in a much higher evaporation temperature for the smallest grains, compared to DL98b, who assume a constant $T_{ev} = 20$ K for all grain sizes. This leads to a decreased damping rate (see discussion at the end of Section 5.1.3) and an increased excitation rate through collisions, and therefore increases the peak frequency of the spectrum.

during thermal spikes. A simple assumption is that in this case ejection occurs after a photon absorption and thermalization of the photon's energy. We take

$$E_\gamma = \frac{\int Q_\nu u_\nu \mathrm{d}\nu}{\int Q_\nu \frac{u_\nu}{h\nu}\mathrm{d}\nu} \tag{56}$$

as the typical energy of an absorbed photon. Typically, $E_\gamma \approx 5$ eV. We then calculate the corresponding grain temperature following DL01: we solve for T_q such that $\bar{E}(T_q) = E_\gamma$, where

$$\bar{E}(T) = \sum_{j=1}^{N_m} \frac{\hbar\omega_j}{\exp(\hbar\omega_j/kT) - 1} \tag{57}$$

is the expectation value of the energy of the grain, and the sum runs over its N_m vibrational degrees of freedom. We take $T_{ev} = \max(T_c, T_q)$ as the evaporation temperature. The result is shown in Fig. 2. One can see that we obtain much higher evaporation temperatures than the ones used by DL98b.[5] The effect may be significant on the final spectrum, as can be seen from Fig. 3.

High-density, low-radiation field case. The previous treatment is valid only if the rate of photon absorption is high enough to eject all stuck species before all available sites on the grain are occupied. We approximate the number of available sites on the grain by the number of superficial C atoms:

$$N_{sites} = \begin{cases} N_C(a) & \text{for cylindrical grains} \\ \frac{3d}{a} N_C(a) & \text{for spherical grains} \end{cases}, \tag{58}$$

where $N_C(a)$ was defined in equation (3) and $d = 3.35$ Å is the interlayer separation in graphite. The ratio of collision rate to photon absorption rate is given by

$$R_{coll/abs} = \frac{n_H\sqrt{8kT/\pi m_H}}{\int Q_\nu \frac{u_\nu}{h\nu}\mathrm{d}\nu\ c} \approx 0.1 \times \frac{n_H}{30\,\mathrm{cm}^{-3}} T_2^{1/2} \chi^{-1} a_{-7}^{-1}. \tag{59}$$

In most environments $R_{coll/abs} \ll N_{sites}$, so there is no accumulation of stuck species. In very dense and dark clouds however, the rate of collisions may become so high compared to the rate of photon absorption that all the sites are occupied. In that case, the assumption that incoming species stick to the grain is no more valid. They will instead bounce off the irregular grain surface. From the fluctuation–dissipation theorem, one expects that, for collisions with neutral species, $F_n = G_n$. Thus, we set the effective evaporation temperature equal to the gas temperature in that case (see equation 74 and discussion below):

$$T_{ev} = T \quad \text{if} \quad R_{coll/abs} > N_{sites}. \tag{60}$$

The actual transition from sticking to elastic collisions should of course be smooth, unlike the discontinuous step we assume here. Our treatment should approximately reflect the physics of collisions except near the transition regime $R_{coll/abs} \sim N_{sites}$.

[5] The mechanism we describe for atomic ejection from grains is called photo-thermo-dissociation (PTD). Rouan et al. (1992) also mention another possible mechanism, photo-dissociation (PD), which is an atomic ejection following the direct interaction of a UV photon with a given C–H bond. PD may lead to even higher ejection temperatures, of the order of 10 000 K.

5.2 Collision with neutral H atoms: neutral grain, general grain shape

We assume that the grain is neutral and has no dipole moment, so there is no interaction whatsoever between the grain and the neutral H atoms (purely geometric cross-section). The phase-space density of incoming H atoms at the grain surface is simply

$$f_{in}(\boldsymbol{v}) = n_H \left(\frac{m_H}{2\pi kT}\right)^{3/2} \mathrm{e}^{-m_H v^2/2kT}, \tag{61}$$

from which one can easily get the excitation rate through incoming particles:

$$\frac{\mathrm{d}\Delta L_z^{2\,(in)}}{\mathrm{d}t\,\mathrm{d}S} = \int v_n (m_H \rho v_\phi)^2 f_{in}(\boldsymbol{v}) \mathrm{d}^3\boldsymbol{v}, \tag{62}$$

where v_n is the component of the velocity normal to the grain surface. This evaluates to

$$\frac{\mathrm{d}\Delta L_z^{2\,(in)}}{\mathrm{d}t\,\mathrm{d}S} = n_H m_H^2 \rho^2 \frac{\pi}{4} \left(\frac{2kT}{\pi m_H}\right)^{3/2}. \tag{63}$$

Integrating over the grain surface, we get

$$\frac{\mathrm{d}\Delta L_z^{2\,(in)}}{\mathrm{d}t} = kT n_H m_H \left(\frac{2kT}{\pi m_H}\right)^{1/2} \frac{4\pi a_{cx}^4}{3}, \tag{64}$$

where $a_{\rm cx}$ was defined in equation (4). For a spherical grain, $a_{\rm cx} = a$. For a disclike grain of thickness d and radius b, spinning around its axis of symmetry, we have

$$a_{\rm cx} = \left[\frac{3}{8}b^3(2d+b)\right]^{1/4}. \tag{65}$$

We can write the excitation rate by incoming H atoms as

$$E^{\rm (in)}_{\parallel,{\rm H}} = \frac{kT}{I\tau_{\rm H}}, \tag{66}$$

where $\tau_{\rm H}$ was defined in equation (24).

The case of evaporating particles is very similar. Assuming the grain surface is at the same temperature T as the gas, the phase-space density of evaporating particles is

$$f_{\rm ev}(\boldsymbol{v}) = n_{\rm H}\left(\frac{m_{\rm H}}{2\pi kT}\right)^{3/2}\exp\left(-\frac{m_{\rm H}(\boldsymbol{v}-\boldsymbol{v}_0)^2}{2kT}\right). \tag{67}$$

In that case, $P_{\rm esc} = 1$ for all outgoing particles. The same calculation therefore leads to

$$E^{\rm (ev)}_{\parallel,{\rm H}} = \frac{kT}{I\tau_{\rm H}} \tag{68}$$

up to terms of order $\mathcal{O}(\Omega^2)$, which comes from the fact that we did not take into account the slight change of ω after the particle has collided (we assumed the same ω for the incoming and the outgoing particle). Detailed balance ensures that

$$\tilde{D}_{\rm H} = \frac{\omega}{\tau_{\rm H}}. \tag{69}$$

Therefore, for non-spherical grains, we will compute collision rates assuming a spherical geometry with radius $a_{\rm cx}$. We just showed that this is an exact result for collisions with neutral H atoms. The collision rates are indeed proportional to the area of the grain, but the angular momentum gained depends on $\langle\rho^2\rangle$, so $a_{\rm cx}$ will approximately reflect both dependencies.

5.3 Collisions with neutral atoms: charged grains

In that case, the incoming neutrals interact with the same potential as the outgoing particles:

$$U(r) = -\frac{1}{2}\alpha\frac{Z_{\rm g}^2 q_{\rm e}^2}{r^4}. \tag{70}$$

We use the same notation as DL98b and define

$$\epsilon_{\rm n} \equiv \sqrt{\frac{mv_{\rm a}^2}{2kT}} \quad \text{and} \quad b_0(v) \equiv a\sqrt{\frac{2v_{\rm a}}{v}}, \tag{71}$$

where $v_{\rm a}$ was defined in equation (40).

We recall, from DL98b, that a trajectory with impact parameter b and velocity at infinity v leads to a collision if

$$b \le b_{\rm max}(v) = \begin{cases} b_0(v) & \text{if} \quad v \le v_{\rm a} \\ a\sqrt{1+v_{\rm a}^2/v^2} & \text{if} \quad v \ge v_{\rm a} \end{cases}. \tag{72}$$

We compute the collision rate

$$\begin{aligned}\frac{{\rm d}N_{\rm coll}}{{\rm d}t} &= n_{\rm n}\int_0^\infty {\rm d}v\, 4\pi v^3 \pi b_{\rm max}^2(v)\left(\frac{m_{\rm n}}{2\pi kT}\right)^{3/2}{\rm e}^{-mv^2/2kT} \\ &= n_{\rm n}2\pi a^2\left(\frac{2kT}{\pi m}\right)^{1/2}\left[{\rm e}^{-\epsilon_{\rm n}^2} + \sqrt{\pi}\epsilon_{\rm n}\,{\rm erf}\,\epsilon_{\rm n}\right].\end{aligned} \tag{73}$$

We can now get the normalized damping and excitation rates for collisions with neutrals:

$$\begin{aligned} F_{\rm n} &= \frac{n_{\rm n}}{n_{\rm H}}\sqrt{\frac{m_{\rm n}}{m_{\rm H}}}\frac{{\rm e}^{-\epsilon_{\rm n}^2}+\sqrt{\pi}\epsilon_{\rm n}\,{\rm erf}\,\epsilon_{\rm n}}{{\rm e}^{-\epsilon_{\rm e}^2}+\sqrt{\pi}\epsilon_{\rm e}\,{\rm erf}\,\epsilon_{\rm e}}\left({\rm e}^{-\epsilon_{\rm e}^2}+2\epsilon_{\rm e}^2\right), \\ G^{\rm (ev)}_{\rm n} &= \frac{T_{\rm ev}}{2T}F_{\rm n} \text{ and} \\ G^{\rm (in)}_{\rm n} &= \frac{n_{\rm n}}{2n_{\rm H}}\sqrt{\frac{m_{\rm n}}{m_{\rm H}}}\left({\rm e}^{-\epsilon_{\rm n}^2}+2\epsilon_{\rm n}^2\right), \end{aligned} \tag{74}$$

where the result for $G^{\rm (in)}_{\rm n}$ is identical to that of DL98b. Note that when $T = T_{\rm ev}$, $G^{\rm (ev)}_{\rm n} = G^{\rm (in)}_{\rm n} = F_{\rm n}/2$, so the principle of detailed balance holds. Moreover, in the case of a neutral grain, if the only rotational excitation and damping process were collisions with neutral species, then the rotational distribution function would be a Maxwellian. In that case, the rotational temperature would be given by $T_{\rm rot} = G_{\rm n}/F_{\rm n}\times T = \frac{1}{2}(T+T_{\rm ev})$, the arithmetic mean of the gas and evaporation temperatures, as was already shown by Purcell (1979).

This is the contribution of an individual neutral for a given grain charge. To get the total contribution, one must average over all grain charges (DL98b showed that the charging time-scale is much shorter than the collision time-scale) and sum over all neutral species, which we take to be atomic and molecular hydrogen, and helium[6] (with $n_{\rm He}/n_{\rm H} = 1/12$).

5.4 Collisions with ions: charged grains

The ion interacts with the grain through the Coulomb, electric dipole and 'image charge' potentials. The latter dominates over the Coulomb potential only in the immediate vicinity of the grain surface, so we will neglect it for charged grains. Properly accounting for it would result in a slight increase in both damping and excitation rates as this is an attractive potential. The general solution for this problem, with a rotating electric dipole moment, is still not analytical. Thus, for simplicity, we will only consider the case where the electric dipole moment can be considered as non-rotating, i.e. when the time-scale of the collision is short compared to the rotation period of the grain. This is justified as, when the ion reaches the vicinity of the grain surface, the ratio of collision time-scale to rotation time-scale is approximately $\omega a/v \sim \sqrt{m_{\rm i}/m_{\rm gr}} \ll 1$. We will assume that the grain is spherical, so that the electric dipole moment is randomly oriented relative to the rotation axis (for cylindrical grains this is not the case but we will assume so for simplicity). Note that when the grain rotates rapidly, the component of the dipole moment perpendicular to the rotation axis averages out, but not the parallel component. Although this problem will be different in nature as this alignment creates anisotropic excitation by collisions, the magnitude of the non-rotating part of the dipole moment will remain of the same order (a factor $1/\sqrt{3}$ smaller only), so our approximation should give a decent idea of what the effect of the dipole moment is on the trajectory.

We assume a spherical geometry with radius $a_{\rm cx}$. Taking $\boldsymbol{\mu}$ as the polar axis for spherical polar coordinates, the interaction potential of the ion in the Coulomb and dipole field of the grain is given by

$$V(r,\theta) = \frac{Z_{\rm g}Z_{\rm i}q_{\rm e}^2}{r} + \frac{Z_{\rm i}q_{\rm e}\mu\cos\theta}{r^2}. \tag{75}$$

[6] Collisions with neutral helium have little effect on the spectrum: the helium contribution dominates $F_{\rm n}$ and $G_{\rm n}$ only in the case where the medium is strongly ionized, i.e. when the dominant rotational excitation and damping mechanisms are rather collisions with ions or plasma drag. We include them for completeness.

The motion in this potential has two obvious constants: the energy E and the angular momentum along the z-axis (along $\boldsymbol{\mu}$), L_z. For this special potential, however, there exists a third constant of the motion. The torque $\dot{\boldsymbol{L}}$ exerted on the ion comes entirely from the second term in the potential and is

$$\dot{\boldsymbol{L}} = -\boldsymbol{r} \times \nabla V(\boldsymbol{r}) = \frac{Z_{\rm i} q_{\rm e} \mu \sin\theta}{r^2} \hat{\boldsymbol{e}}_\phi. \tag{76}$$

Since the azimuthal component of angular momentum is $\boldsymbol{L} \cdot \hat{\boldsymbol{e}}_\phi = mr^2\dot{\theta}$, we can then determine the overall rate of change of the angular momentum:

$$\frac{\rm d}{{\rm d}t}(L^2) = 2m_{\rm i} Z_{\rm i} q_{\rm e} \mu \sin\theta\, \dot{\theta} = -2m_{\rm i} Z_{\rm i} q_{\rm e} \mu \frac{\rm d}{{\rm d}t} \cos\theta. \tag{77}$$

Therefore, we find the constant of the motion[7]

$$\mathcal{A} \equiv L^2 + 2m_{\rm i} Z_{\rm i} q_{\rm e} \mu \cos\theta. \tag{78}$$

Its value can be determined by taking the incoming trajectory at infinity with approach angle θ_∞,

$$\mathcal{A} = (m_{\rm i} b v)^2 + 2m_{\rm i} Z_{\rm i} q_{\rm e} \mu \cos\theta_\infty. \tag{79}$$

The energy of the trajectory is

$$\frac{1}{2} m_{\rm i} \dot{r}^2 + V_{\rm eff}(r) = E, \tag{80}$$

where $V_{\rm eff}(r)$ is the sum of the potential $V(r, \theta)$ and the tangential kinetic energy $L^2/2m_{\rm i}\, r^2$:

$$V_{\rm eff}(r) \equiv \frac{Z_{\rm g} Z_{\rm i} q_{\rm e}^2}{r} + \frac{m_{\rm i}(bv)^2 + 2Z_{\rm i} q_{\rm e} \mu \cos\theta_\infty}{2r^2}. \tag{81}$$

It is easier to work with the following dimensionless parameters:

$$\psi \equiv \frac{Z_{\rm g} Z_{\rm i} q_{\rm e}^2}{a_{\rm cx} kT}, \quad \tilde{\mu} \equiv \frac{Z_{\rm i} q_{\rm e} \mu}{a_{\rm cx}^2 kT}. \tag{82}$$

Their physical meaning is as follows : $|\psi| \ll 1$ when the thermal energy of the ion dominates over the electrostatic interaction energy and $|\psi| \gg 1$ when the electrostatic interaction dominates. The sign determines whether the interaction is attractive ($\psi < 0$) or repulsive ($\psi > 0$). $\tilde{\mu}$ is the equivalent quantity for the dipole interaction. Note that we consider only positively charged ions so $\tilde{\mu} > 0$. We also work with the dimensionless variables

$$c = \frac{b}{a_{\rm cx}}, u = \sqrt{\frac{m_{\rm i}}{2kT}} v. \tag{83}$$

The effective potential can now be written as

$$V_{\rm eff}(r) = kT \left[\psi \frac{a_{\rm cx}}{r} + \left(u^2 c^2 + \tilde{\mu} \cos\theta_\infty\right) \left(\frac{a_{\rm cx}}{r}\right)^2 \right]. \tag{84}$$

A study of this potential leads to the following condition for collision:

$$\cos\theta_\infty < X_{\rm max}(c, u) \equiv \tilde{\mu}^{-1} \left(u^2 - u^2 c^2 - \psi\right). \tag{85}$$

Note that if $X_{\rm max} < -1$, then there is never collision for any angle. If $X_{\rm max} > 1$, then all angles lead to a collision. We define

$$X(c, u) \equiv \max\left\{-1, \min\left[1, X_{\rm max}(c, u)\right]\right\}. \tag{86}$$

[7] This may also be derived by the Hamilton–Jacobi method in spherical polar coordinates.

Now, we can compute the collision rate

$$\begin{aligned} \frac{{\rm d}N_{\rm coll}}{{\rm d}t} &= n_{\rm i} \int 2\pi v^3 {\rm d}v\, 2\pi b {\rm d}b \left(\frac{m_{\rm i}}{2\pi kT}\right)^{3/2} \\ &\quad \times {\rm e}^{-m_{\rm i} v^2/2kT} (X+1) \\ &= 2n_{\rm i} \sqrt{\frac{2\pi kT}{m_{\rm i}}} a_{\rm cx}^2 \\ &\quad \times \int 2u^3 {\rm e}^{-u^2} {\rm d}u 2c {\rm d}c \frac{X+1}{2}. \end{aligned} \tag{87}$$

We can also get the excitation rate by incoming ions

$$\begin{aligned} \frac{{\rm d}\Delta L_z^2}{{\rm d}t} &= n_{\rm i} \int \frac{(mbv)^2}{3} 2\pi v^3 {\rm d}v\, 2\pi b {\rm d}b \left(\frac{m_{\rm i}}{2\pi kT}\right)^{3/2} \\ &\quad \times {\rm e}^{-m_{\rm i} v^2/2kT} (X+1) \\ &= \frac{2n_{\rm i} m_{\rm i}^2 a_{\rm cx}^4}{3\pi} \left(\frac{2\pi kT}{m_{\rm i}}\right)^{3/2} \\ &\quad \times \int u^5 {\rm e}^{-u^2} {\rm d}u 4c^3 {\rm d}c \frac{X+1}{2}. \end{aligned} \tag{88}$$

These integrals can be evaluated explicitely and one then gets, for the charged grains $Z_{\rm g} \neq 0$,

$$\begin{aligned} F_{\rm i}(Z_{\rm g} \neq 0) &= \frac{n_{\rm i}}{n_{\rm H}} \sqrt{\frac{m_{\rm i}}{m_{\rm H}}} \frac{{\rm e}^{-\epsilon_{\rm i}^2} + 2\epsilon_{\rm i}^2}{{\rm e}^{-\epsilon_{\rm i}^2} + \sqrt{\pi}\epsilon_{\rm i}\, {\rm erf}\, \epsilon_{\rm i}} g_1(\psi, \tilde{\mu}), \\ G_{\rm i}^{\rm (ev)}(Z_{\rm g} \neq 0) &= \frac{T_{\rm ev}}{2T} F_{\rm i}(Z_{\rm g} \neq 0) \quad \text{and} \\ G_{\rm i}^{\rm (in)}(Z_{\rm g} \neq 0) &= \frac{n_{\rm i}}{2n_{\rm H}} \sqrt{\frac{m_{\rm i}}{m_{\rm H}}} g_2(\psi, \tilde{\mu}), \end{aligned} \tag{89}$$

where we have defined $g_1(\psi, \tilde{\mu}) =$

$$\begin{cases} \begin{cases} 1 - \psi & \psi < 0 \\ {\rm e}^{-\psi} \sinh\tilde{\mu}/\tilde{\mu} & \psi > 0 \end{cases}, \tilde{\mu} \leq |\psi| \\ \dfrac{1 - {\rm e}^{-(\psi+\tilde{\mu})} + \tilde{\mu} - \psi + \frac{1}{2}(\tilde{\mu} - \psi)^2}{2\tilde{\mu}}, \tilde{\mu} > |\psi|, \end{cases} \tag{90}$$

and $g_2(\psi, \tilde{\mu}) =$

$$\begin{cases} \begin{cases} 1 - \psi + \psi^2/2 + \tilde{\mu}^2/6 & \psi < 0 \\ {\rm e}^{-\psi} \sinh\tilde{\mu}/\tilde{\mu} & \psi > 0 \end{cases}, \tilde{\mu} \leq |\psi| \\ \dfrac{1 - {\rm e}^{-(\psi+\tilde{\mu})} + \tilde{\mu} - \psi + \frac{1}{2}(\tilde{\mu} - \psi)^2 + \frac{1}{6}(\tilde{\mu} - \psi)^3}{2\tilde{\mu}}, \tilde{\mu} > |\psi|. \end{cases} \tag{91}$$

Note that these functions coincide with the functions $g_1(\psi)$ and $g_2(\psi)$ defined in DL98b for $\tilde{\mu} = 0$. We also defined $\epsilon_{\rm i}^2 \equiv Z_{\rm g}^2 q_{\rm e}^2 \alpha_{\rm i}/2a^4 kT_{\rm ev}$ (here, $\alpha_{\rm i}$ is the polarizability of species i after it neutralizes on the grain surface, e.g. when considering collisions with the C^+ ion, we take the polarizability of the neutral C atom). Note that even when $T_{\rm ev} = T$, $F_{\rm i} \neq G_{\rm i}$ as the incoming and outgoing particles are in different ionization states; detailed balance does not apply since realistic ISM phases are not in Saha equilibrium. Numerically, one has (with $T_2 \equiv T/100\,{\rm K}$)

$$\psi \approx 170 Z_{\rm g} a_{-7}^{-1} T_2^{-1} \tag{92}$$

and

$$\tilde{\mu} \approx 30 \frac{\langle \mu^2 \rangle^{1/2}|_{10^{-7}\,{\rm cm}}}{9.3\,{\rm debye}} a_{-7}^{-1/2} T_2^{-1}. \tag{93}$$

From these values, one can see that in general the effect of the dipole moment cannot be neglected a priori, as $\tilde{\mu}$ is not small compared to unity. However, in general $\tilde{\mu} < |\psi|$. This implies that, for negatively charged grains, the dipole moment has little or no

effect on the excitation and damping rate. For positively charged grains, the damping and excitation rate are both increased by the huge factor $\sinh\tilde{\mu}/\tilde{\mu}$, but still remain extremely small due to the Coulomb repulsion, which shows in the factor $\mathrm{e}^{-\psi}$.

We therefore conclude that DL98b approximation of neglecting the effect of the electric dipole moment on the trajectory of ions is essentially valid in the case of collisions with charged grains. It has only a significant effect for positively charged grains, for which the Coulomb repulsion implies an extremely small rate of collisions with ions anyway. We still account for the electric dipole moment for the sake of completeness.

5.5 Collisions with ions, neutral grain

In that case, the Coulomb potential vanishes and the 'image charge' potential has to be taken into account. We carry the calculation using the same assumptions as in the previous section: slowly rotating spherical grain, with radius $a_{\rm cx}$. Taking $\boldsymbol{\mu}$ as the polar axis for spherical polar coordinates, the interaction potential of the ion in the dipole and induced dipole field of the grain is given by

$$V(r,\theta) = -\frac{Z_{\rm i}^2 q_{\rm e}^2 a_{\rm cx}^3}{2r^2(r^2-a_{\rm cx}^2)} + \frac{Z_{\rm i} q_{\rm e}\mu\cos\theta}{r^2}. \tag{94}$$

The considerations that lead to the third constant of motion $\mathcal{A}$ hold again. The energy of the trajectory is

$$\frac{1}{2}m\dot{r}^2 + V_{\rm eff}(r) = E, \tag{95}$$

where $V_{\rm eff}(r)$ is given by

$$V_{\rm eff}(r) \equiv -\frac{Z_{\rm i}^2 q_{\rm e}^2 a^3}{2r^2(r^2-a^2)} + \frac{m(bv)^2 + 2Z_{\rm i} q_{\rm e}\mu\cos\theta_\infty}{2r^2}. \tag{96}$$

Following DL98b, we define the dimensionless parameter

$$\phi^2 \equiv \frac{2Z_{\rm i}^2 q_{\rm e}^2}{a_{\rm cx} kT}, \tag{97}$$

which describes whether the image charge attraction dominates over the thermal energy ($\phi \gg 1$) or the thermal energy dominates ($\phi \ll 1$). The effective potential can be written

$$V_{\rm eff}(r) = kT\left[-\frac{\phi^2 a_{\rm cx}^4}{4r^2(r^2-a_{\rm cx}^2)} + \left(u^2c^2 + \tilde{\mu}\cos\theta_\infty\right)\left(\frac{a_{\rm cx}}{r}\right)^2\right], \tag{98}$$

where $\tilde{\mu}$, c and u were defined in equations (82) and (83).

A study of this potential leads to the following condition for collision:

$$\cos\theta_\infty < X_{\rm max}(c,u) \equiv \tilde{\mu}^{-1}\left(u^2 - u^2c^2 + \phi u\right). \tag{99}$$

The collision and excitation rates are obtained as in equations (86), (87) and (88). One can then obtain the normalized damping and excitation rates for collisions of ions with a neutral grain:

$$F_{\rm i}(Z_{\rm g}=0) = \frac{n_{\rm i}}{n_{\rm H}}\sqrt{\frac{m_{\rm i}}{m_{\rm H}}}h_1(\phi,\tilde{\mu}), \tag{100}$$

$$G_{\rm i}^{\rm (ev)}(Z_{\rm g}=0) = \frac{T_{\rm ev}}{2T}F_{\rm i}(Z_{\rm g}=0), \tag{101}$$

$$G_{\rm i}^{\rm (in)}(Z_{\rm g}=0) = \frac{n_{\rm i}}{2n_{\rm H}}\sqrt{\frac{m_{\rm i}}{m_{\rm H}}}h_2(\phi,\tilde{\mu}), \tag{102}$$

where we have defined

$$h_1(\phi,\tilde{\mu}) \equiv \frac{1}{2} + \frac{\tilde{\mu}}{4} + \frac{2+\phi^2}{4\tilde{\mu}}\left(1-\mathrm{e}^{-u_0^2}\right) - \frac{\phi u_0}{4\tilde{\mu}}\mathrm{e}^{-u_0^2} + \frac{\pi^{1/2}\phi}{2}\left(1+\frac{3-2\tilde{\mu}}{4\tilde{\mu}}\,\mathrm{erf}\,u_0\right), \tag{103}$$

$$h_2(\phi,\tilde{\mu}) \equiv \frac{1}{2} + \frac{3\pi^{1/2}}{4}\phi + \frac{\phi^2}{4} + \frac{\tilde{\mu}^2}{12} + \frac{\tilde{\mu}}{4} + \frac{1+\phi^2}{2\tilde{\mu}}(1-\mathrm{e}^{-u_0^2}) + \frac{2\tilde{\mu}\phi^2 + \phi(2\tilde{\mu}-7)u_0}{16\tilde{\mu}}\mathrm{e}^{-u_0^2} + \frac{\pi^{1/2}\phi}{32\tilde{\mu}}\left(4\tilde{\mu}^2 - 12\tilde{\mu} + 15 + 2\phi^2\right)\mathrm{erf}\,u_0 \tag{104}$$

and

$$u_0 \equiv \frac{-\phi + \sqrt{\phi^2+4\tilde{\mu}}}{2}. \tag{105}$$

Note that in the limit $\tilde{\mu}\to 0$, we recover DL98b result as

$$h_1(\phi,\tilde{\mu}\to 0) = 1 + \frac{\pi^{1/2}}{2}\phi + \mathcal{O}(\tilde{\mu}^3), \tag{106}$$

$$h_2(\phi,\tilde{\mu}\to 0) = 1 + \frac{3\pi^{1/2}}{4}\phi + \frac{\phi^2}{2} + \mathcal{O}(\tilde{\mu}^2). \tag{107}$$

However, the parameter $\tilde{\mu}$ is not small in general, as we saw in equation (93), so the effect of the dipole moment on the trajectory cannot be neglected. Note that we also have $\phi \approx 18\, a_{-7}^{-1/2}\, T_2^{-1/2}$. The net effect of the dipole moment is to increase the collision and excitation rates, as can be seen from Fig. 4. In contrast to the case of charged grains, the electric dipole moment does have a significant effect and cannot be discarded.

The effect of the dipole moment is always to increase both the collision and excitation rates, for both charged and neutral grains. This can be understood as follows. When the dipole moment vanishes, ions with a given velocity at infinity v collide with the grain if their impact parameter is such that $b < b_{\rm max}(v)$. The effect of the dipole moment is to make a smooth transition from non-colliding to colliding trajectories: all ions with impact parameter $b < b_1(v)$ collide with the grain, a fraction $[X(b,v)+1]/2$ of those for which $b_1(v) < b < b_2(v)$ do collide, and none of the ions with $b > b_2(v)$ collide. b_1 and b_2 are such that $b_1 < b_{\rm max} < b_2$. As a result, a fraction of trajectories for which $b_1(v) < b < b_{\rm max}(v)$ do not lead to collision anymore (compared to the vanishing dipole case), and a fraction of trajectories $b_{\rm max}(v) < b < b_2(v)$ now lead to collision. The suppressed colliding trajectories have a lower rate of collision and angular momentum than the added colliding trajectories. Thus, the net effect of the dipole moment is to increase the collision and rotational excitation rates.

6 PLASMA DRAG

DL98b computed the effect of torques from passing ions on the electric dipole moments of the dust grains, which they named 'plasma drag'. They computed this effect for straight line trajectories (the 'Born approximation'). Here, we include the full hyperbolic trajectory in the case of charged grains. We also account for the rotation of the grain explicitly. Moreover, we do not include trajectories leading to collisions, as they will give away their entire angular momentum through collision, which we already accounted for. A precise calculation is important because plasma drag is one of the major excitation processes in some environments. Note that treatments of the plasma drag effect that treat the plasma as a linear

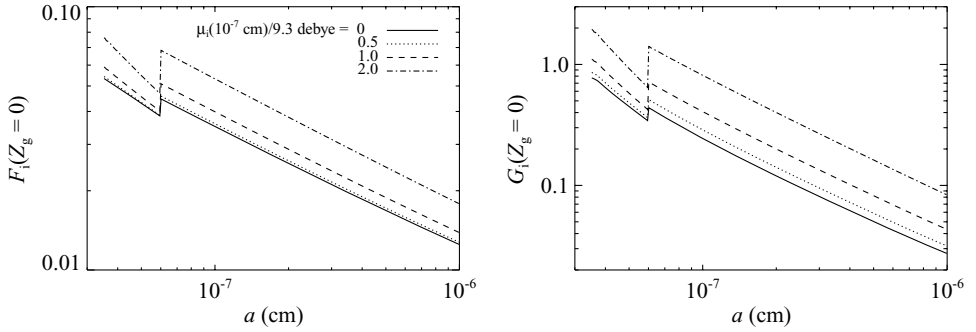

Figure 4. $F_i(Z_g = 0)$ (left-hand panel) and $G_i(Z_g = 0)$ (right-hand panel) for several values of the electric dipole moment, in CNM conditions, equation (162).

dielectric medium (Ragot 2002) with the drag due to the imaginary part of the dielectric constant $\Im\,\epsilon(\omega, k)$ implicitly assume the Born approximation and do not capture the effects considered here.

We will find that the straight line approximation usually overestimates the plasma drag. In the case of positively charged grains, there is a range of impact parameters where the ion trajectory is deflected away from the grain, thereby suppressing angular momentum transfer. For negatively charged grains, ions can be focused by electrostatic attraction. Anderson & Watson (1993) argued that this is not a significant correction because the increased torque during close approach balances the shorter interaction time since the ion gains kinetic energy as it is attracted to the grain; however, we will see that in these cases there is a cancellation of angular momentum transfer in different parts of the trajectory that leads to reduced drag. For very special cases, the grain can corotate with the ion during close approach leading to an enhancement of the plasma drag, but this occurs for only a narrow range of impact parameters and does not compensate for the reduction of plasma drag that we find in other regimes.

As in DL98b, we find it the easiest to directly compute the plasma excitation G_p and use the fluctuation–dissipation theorem to infer $F_p = G_p$.

6.1 Charged grain

We consider the trajectories of positively charged ion (charge $Z_i > 0$) in the electric potential of a charged dust grain (charge $Z_g \neq 0$). The trajectories are not strictly hyperbolic due to the presence of the electric dipole potential (see Section 5.4). However, we saw that it has little influence on collisions and we will neglect its effect on the trajectory here, assuming they are hyperbolic and determined by the Coulomb potential only. The eccentricity of the hyperbolic trajectory of the ion will be denoted e (as opposed to the elementary charge q_e).

Let the ion trajectory (a hyperbola) be in the $(\hat{\boldsymbol{e}}_y, \hat{\boldsymbol{e}}_z)$ plane, symmetric about the $\hat{\boldsymbol{e}}_y$ axis. The ion position is given by

$$\boldsymbol{r} = r\hat{\boldsymbol{e}}_r = r(\alpha)\left(\cos\alpha\,\hat{\boldsymbol{e}}_y + \sin\alpha\,\hat{\boldsymbol{e}}_z\right). \tag{108}$$

The hyperbolic trajectory of impact parameter b and velocity at infinity v can be described in polar coordinates as

$$\begin{aligned} r(\alpha) &= \frac{p}{e\cos\alpha - 1} \quad \alpha \in (-\alpha_e, \alpha_e) \qquad (Z_g > 0), \\ r(\alpha) &= \frac{p}{1 - e\cos\alpha} \quad \alpha \in (\alpha_e, 2\pi - \alpha_e)\ (Z_g < 0); \end{aligned} \tag{109}$$

the eccentricity and semilatus rectum[8] of the trajectory are

$$e = \sqrt{1 + \left(\frac{m_i b v^2}{Z_i Z_g q_e^2}\right)^2} \quad \text{and} \quad p = b\sqrt{e^2 - 1}. \tag{110}$$

The range of longitudes α of the trajectory are determined by the limiting case

$$\alpha_e \equiv \arccos\frac{1}{e}. \tag{111}$$

The longitude can be related to the true anomaly f familiar from planetary dynamics by $\alpha = f$ for repulsive ($Z_g > 0$) cases and $\alpha = \pi + f$ for attractive ($Z_g < 0$) cases. We will need the following expression for the time $t(\alpha)$, valid in both cases (for the case of an attractive potential, see e.g. Geyling & Westerman 1971, equation 2.4.12):

$$t(\alpha) = \frac{b}{v}\frac{1}{e+1}\left[\sqrt{\frac{e+1}{e-1}}\ln\left|\frac{\tan\frac{\alpha}{2} + \sqrt{\frac{e-1}{e+1}}}{\tan\frac{\alpha}{2} - \sqrt{\frac{e-1}{e+1}}}\right| - \frac{2e\tan\frac{\alpha}{2}}{\tan^2\frac{\alpha}{2} - \frac{e-1}{e+1}}\right]. \tag{112}$$

In order to characterize the torque on the grain, we must first take the unit vector in the direction of grain rotation,

$$\hat{\boldsymbol{e}}_\omega = \sin\theta\cos\phi\,\hat{\boldsymbol{e}}_x + \sin\theta\sin\phi\,\hat{\boldsymbol{e}}_y + \cos\theta\,\hat{\boldsymbol{e}}_z, \tag{113}$$

so that $\boldsymbol{\omega} = \omega\hat{\boldsymbol{e}}_\omega$. We use (θ, ϕ) to parametrize the (general) direction of rotation. We define the other two axes:

$$\begin{aligned} \hat{\boldsymbol{e}}_\theta &= \cos\theta\cos\phi\,\hat{\boldsymbol{e}}_x + \cos\theta\sin\phi\,\hat{\boldsymbol{e}}_y - \sin\theta\,\hat{\boldsymbol{e}}_z \quad \text{and} \\ \hat{\boldsymbol{e}}_\phi &= -\sin\phi\,\hat{\boldsymbol{e}}_x + \cos\phi\,\hat{\boldsymbol{e}}_y. \end{aligned} \tag{114}$$

In this system, the electric dipole moment of the grain is

$$\boldsymbol{\mu} = \mu_\parallel\hat{\boldsymbol{e}}_\omega + \mu_\perp\left[\cos(\omega t + \chi)\hat{\boldsymbol{e}}_\theta + \sin(\omega t + \chi)\hat{\boldsymbol{e}}_\phi\right], \tag{115}$$

where $t = 0$ is taken to be the time when the ion is at the closest approach (i.e. $\boldsymbol{r} \parallel \hat{\boldsymbol{e}}_y$) and $\chi \in [0, 2\pi)$ is the random angle that $\boldsymbol{\mu}_\perp$ makes with $\hat{\boldsymbol{e}}_\theta$ at that time.

The ion electric field exerts a torque on the grain dipole moment:

$$I\frac{\mathrm{d}\boldsymbol{\omega}}{\mathrm{d}t} = \boldsymbol{\mu}\times\boldsymbol{E} = -I\frac{Z_i q_e}{r^2}\boldsymbol{\mu}\times\hat{\boldsymbol{e}}_r. \tag{116}$$

[8] The positive and negative cases of equation (109) could have been unified by taking the negative branches of the square root in equation (110), however we have not taken this route.

Using the conservation of angular momentum, $r^2\dot{\alpha} = bv$, we can rewrite

$$\frac{\mathrm{d}\boldsymbol{\omega}}{\mathrm{d}\alpha} = -\frac{Z_\mathrm{i} q_\mathrm{e}}{Ibv}\boldsymbol{\mu}\times\hat{\boldsymbol{e}}_\mathrm{r}. \tag{117}$$

We project that along the direction of $\hat{\boldsymbol{e}}_\omega$

$$\frac{\mathrm{d}\omega_\parallel}{\mathrm{d}\alpha} = -\frac{Z_\mathrm{i} q_\mathrm{e}\mu_\perp}{Ibv}\Big[\cos(\omega t+\chi)\cos\alpha\cos\phi - \sin(\omega t+\chi)(\cos\alpha\cos\theta\sin\phi - \sin\alpha\sin\theta)\Big]. \tag{118}$$

Expanding the sines and cosines, we integrate over the trajectory. We keep only the parts of the integral for which the inbound and outbound parts do not cancel, i.e. those which are even under $\alpha\rightarrow -\alpha$ ($Z_\mathrm{g}>0$) or $\alpha\rightarrow 2\pi-\alpha$ ($Z_\mathrm{g}<0$); note that $t(\alpha)$ is even. We are then left with

$$\delta\omega_\parallel = \frac{Z_\mathrm{i} q_\mathrm{e}\mu_\perp}{Ibv}\Big[(\sin\chi\cos\theta\sin\phi - \cos\chi\cos\phi)\times\int\cos\omega t\cos\alpha\mathrm{d}\alpha - \cos\chi\sin\theta\int\sin\omega t\sin\alpha\mathrm{d}\alpha\Big]. \tag{119}$$

In order to find the plasma excitation coefficient, we need to sum $\delta\omega_\parallel^2$ over collisions. We begin by averaging $\delta\omega_\parallel^2$ over solid angles for (θ,ϕ) and over angles for χ. The result is

$$\langle\delta\omega_\parallel^2\rangle = \frac{1}{3}\left(\frac{2Z_\mathrm{i} q_\mathrm{e}\mu_\perp}{Ibv}\right)^2\mathcal{I}\left(\frac{\omega b}{v},e,Z_\mathrm{g}\right). \tag{120}$$

We have defined the integral

$$\mathcal{I}\left(\frac{\omega b}{v},e,Z_\mathrm{g}\right) \equiv \left(\int\cos\omega t\cos\alpha\mathrm{d}\alpha\right)^2 + \left(\int\sin\omega t\sin\alpha\mathrm{d}\alpha\right)^2, \tag{121}$$

where the integration limits are given by $0<\alpha<\alpha_\mathrm{e}(Z_\mathrm{g}>0)$ or $\alpha_\mathrm{e}<\alpha<\pi$ ($Z_\mathrm{g}<0$). Note that $\mathcal{I}$ only integrates over the inbound part of the trajectory; the outbound part is equal by symmetry.

The excitation rate due to plasma drag is then given by

$$\frac{\mathrm{d}\Delta\omega_\parallel^2}{\mathrm{d}t} = \int_0^\infty\mathrm{d}v\int_{b_\mathrm{max}(v)}^\infty 2\pi b\,\mathrm{d}b\,n_\mathrm{i}\,4\pi v^3 \times\left(\frac{m_\mathrm{i}}{2\pi kT}\right)^{3/2}\mathrm{e}^{-m_\mathrm{i}v^2/2kT}\frac{1}{3}\left(\frac{2Z_\mathrm{i} q_\mathrm{e}\mu_\perp}{Ibv}\right)^2 \times\mathcal{I}\left(\frac{\omega b}{v},e,Z_\mathrm{g}\right), \tag{122}$$

where $b_\mathrm{max}(v)$, the maximum impact parameter for collision to occur, is defined as

$$b_\mathrm{max}(v) = \begin{cases} 0 & mv^2/2kT\le\psi \\ a_\mathrm{cx}\sqrt{1-(2kT/mv^2)\psi} & mv^2/2kT>\psi\end{cases}, \tag{123}$$

where $\psi = Z_\mathrm{g}Z_\mathrm{i}q_\mathrm{e}^2/a_\mathrm{cx}kT$.

Note that technically the integration over impact parameters should stop at the Debye length

$$\lambda_\mathrm{D} = \sqrt{\frac{kT}{4\pi n_\mathrm{e}q_\mathrm{e}^2}} \approx 398\left(\frac{T_2}{n_\mathrm{e}/0.03\,\mathrm{cm}^{-3}}\right)^{1/2}. \tag{124}$$

However, we will see below that the integrand vanishes exponentially for

$$b>v/\omega \approx 4.5\times10^{-6}a_{-7}^{5/2}\sqrt{\frac{m_\mathrm{H}}{m_\mathrm{i}}}\frac{v}{v_\mathrm{th}}\frac{\omega_\mathrm{th}}{\omega}\,\mathrm{cm} \tag{125}$$

which is much smaller than the Debye length. Converting this into an excitation coefficient, we find

$$G_\mathrm{p} = \frac{n_\mathrm{i}}{n_\mathrm{H}}\sqrt{\frac{m_\mathrm{i}}{m_\mathrm{H}}}\left(\frac{Z_\mathrm{i} q_\mathrm{e}\mu_\perp}{a_\mathrm{cx}^2kT}\right)^2\times g_\mathrm{p}\left(\psi,\sqrt{\frac{m_\mathrm{i}a_\mathrm{cx}^2}{2kT}}\omega\right), \tag{126}$$

where

$$g_\mathrm{p}(\psi,\Omega) \equiv \int_0^\infty 2u\mathrm{e}^{-u^2}\mathrm{d}u\int_{\frac{b_\mathrm{max}}{a_\mathrm{cx}}}^\infty\frac{\mathrm{d}c}{c}\mathcal{I}\left(\frac{\Omega c}{u},e,Z_\mathrm{g}\right), \tag{127}$$

where the eccentricity is given by

$$e = \sqrt{1+\left(\frac{2cu^2}{\psi}\right)^2}. \tag{128}$$

Note that we recover DL98b result[9] in the limit $\mathcal{I}=1$.

This expression has to be averaged over the grain charge and summed over all present ions.

Straight line limit for $\mathcal{I}$. In the limit $e\rightarrow\infty$, it is easier to express the integrals as a function of time, using

$$\cos\alpha = \frac{y}{\sqrt{y^2+z^2}} = \frac{b}{\sqrt{b^2+(vt)^2}},\quad \sin\alpha = \frac{vt}{\sqrt{b^2+(vt)^2}}\quad\text{and}\quad \mathrm{d}\alpha = \frac{1}{1+\left(\frac{vt}{b}\right)^2}\frac{v}{b}\mathrm{d}t. \tag{129}$$

In this case, the first function for $\mathcal{I}$ reduces to

$$\int\cos\omega t\cos\alpha\,\mathrm{d}\alpha = \frac{v}{b}\int_0^\infty\frac{\cos\omega t\,\mathrm{d}t}{[1+(vt/b)^2]^{3/2}} = \frac{\omega b}{v}K_1\left(\frac{\omega b}{v}\right), \tag{130}$$

where K_1 is a modified Bessel function of the second kind. (Here, we used equation 9.6.25 of Abramowitz & Stegun 1972 with $\nu=1$, $z=1$ and $x=\omega\,b/v$.) The other integral is

$$\int\sin\omega t\sin\alpha\,\mathrm{d}\alpha = \frac{v}{b}\int_0^\infty\frac{vt}{b}\frac{\sin\omega t}{[1+(vt/b)^2]^{3/2}}\mathrm{d}t = \int_0^\infty\frac{\tau\sin x\tau\,\mathrm{d}\tau}{(1+\tau^2)^{3/2}}, \tag{131}$$

where $x=\omega\,b/v$. Since $\tau(1+\tau^2)^{-3/2}$ is the derivative of $-(1+\tau^2)^{-1/2}$, we can integrate by parts and find

$$\frac{-\sin x\tau}{\sqrt{1+\tau^2}}\bigg|_0^\infty + \int_0^\infty\frac{x\cos x\tau\,\mathrm{d}\tau}{\sqrt{1+\tau^2}}. \tag{132}$$

The boundary terms evaluate to zero, and the second integral can again be evaluated to $xK_0(x)$ using equation (9.6.25) of Abramowitz & Stegun (1972) with $\nu=0$ and $z=1$. Thus, we have

$$\mathcal{I} = x^2[K_0^2(x)+K_1^2(x)],\quad x=\frac{\omega b}{v}. \tag{133}$$

Note that when $\omega\rightarrow0$, we recover DL98b result, i.e.

$$\mathcal{I}\left(\frac{\omega b}{v}=0,e\rightarrow\infty,Z_\mathrm{g}\right) = 1. \tag{134}$$

We moreover have an exact functional shape for the cut-off at large rotation rates.

[9] DL98b include a term due to the parallel component of $\boldsymbol{\mu}$ which is not relevant as it only leads to excitation perpendicular to $\boldsymbol{\omega}$.

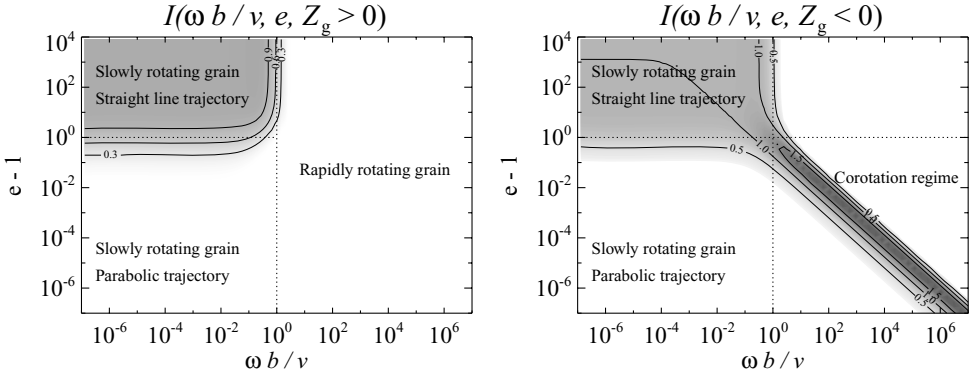

Figure 5. Contour levels of $\mathcal{I}(\frac{\omega b}{v}, e, Z_g > 0)$ (left-hand panel) and $\mathcal{I}(\frac{\omega b}{v}, e, Z_g < 0)$ (right-hand panel). Both show that $\mathcal{I}$ goes to unity for slowly rotating grain, straight line trajectories and vanishes for rapidly rotating grains or nearly parabolic trajectory. In the case of negatively charged grains, though, there is a visible corotation regime, where $e - 1 \ll 1$ and $\omega\, b/v\, (e-1) \sim 1$, for which the ion and the grain approximately corotate, enhancing the torque given to the grain.

Non rotating grain limit for $\mathcal{I}$. It is straightforward to show that

$$\mathcal{I}\left(\frac{\omega b}{v} = 0, e\right) = 1 - \frac{1}{e^2} \tag{135}$$

for both positively and negatively charged grains. Thus, the nearly parabolic trajectories $e - 1 \ll 1$ are suppressed by a factor $\sim 2(e-1)$.

The numerical calculation of $\mathcal{I}$ in the general case is tricky because it involves integrating an oscillating function which frequency goes to infinity at one limit of the integral, as $t(\alpha \to \alpha_e) \to \infty$. We refer the reader to Appendix A for the description of the method used for numerical computation. Fig. 5 shows the resulting dimensionless torques. An important feature is that for negatively charged grains, ions with nearly parabolic trajectories may corotate with the grain which results in an enhanced torque.

6.2 Neutral grain

The exact calculation of the trajectory in the electric dipole potential and the 'image charge potential' is untractable analytically, and would require a heavy numerical calculation. Therefore, we will make the following simplifications. First, we neglect the effect of the electric dipole moment on the trajectory. This assumption is somewhat cavalier, as we saw previously that the electric dipole moment may significantly affect the ion trajectory in the case of a neutral grain. Furthermore, although trajectories in the 'image charge potential' will be curved in general, we will consider them to be straight lines. Thus, we will approximate the torque given to the grain by equation (120), where $\mathcal{I}$ is given by equation (133). Colliding trajectories should not be taken into account for the plasma drag excitation rate. Thus, we integrate the torque only over trajectories with impact parameter $b > b_{\max}(v)$, with

$$b_{\max} = a_{\rm cx}\sqrt{1 + \frac{\phi}{u}} \tag{136}$$

(see DL98b equation B24 and the definition of ϕ equation 97).

Therefore, in the case of neutral grains, we have

$$G_{\rm p}(Z_g = 0) = \frac{n_{\rm i}}{n_{\rm H}}\sqrt{\frac{m_{\rm i}}{m_{\rm H}}}\left(\frac{Z_{\rm i} q_e \mu_\perp}{a_{\rm cx}^2 kT}\right)^2 \times \tilde{g}_{\rm p}\left(\phi, \sqrt{\frac{m_{\rm i} a_{\rm cx}^2}{2kT}}\omega\right), \tag{137}$$

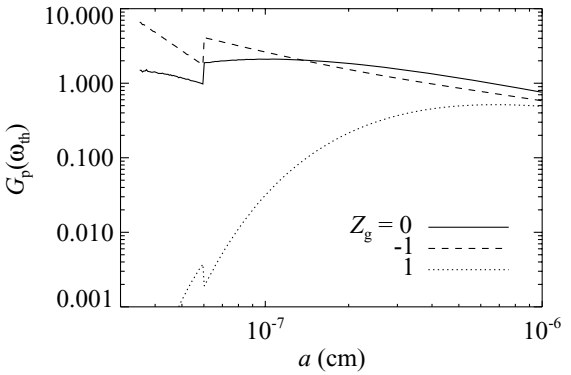

Figure 6. Normalized excitation rate due to plasma drag $G_{\rm p}(\omega_{\rm th})$ for a neutral grain, a positively charged grain and a negatively charged grain in CNM conditions (equation 162), evaluated at the 'thermal rotation rate' $\omega_{\rm th} = (2kT/I)^{1/2}$. All of them are lower than estimated by DL98b. It is clear that the positively charged grains are much less excited than the neutral and negatively charged grains. The kink at 6 Å is due to the change of grain shape.

where

$$\tilde{g}_{\rm p}(\phi, \Omega) \equiv \int_0^\infty 2u e^{-u^2} {\rm d}u \int_{\frac{b_{\max}}{a_{\rm cx}}}^\infty \frac{{\rm d}c}{c}\,\mathcal{I}\left(\frac{\Omega c}{u}, e \to \infty\right). \tag{138}$$

The normalized excitation rate for plasma drag for CNM conditions (equation 162) is shown in Fig. 6.

7 INFRARED EMISSION

A dust grain absorbs light and re-emits it in the infrared. A rotating grain will also radiate angular momentum, which damps its rotation.

DL98b compute this damping rate by modelling the grain as composed of six rotating dipoles. We give here a more accurate calculation, using the correlation functions of the dipole moment in the grain frame. Our result is a factor of two greater than that of DL98b. We present a classical calculation in this section; the quantum calculation is presented in Appendix B and gives the same result.

The rates of emission of energy and of angular momentum by a varying electric dipole moment:

$$\dot{E} = \frac{2}{3c^3}\ddot{\boldsymbol{p}}^2 \quad \text{and} \quad \dot{\boldsymbol{L}} = \frac{2}{3c^3}\dot{\boldsymbol{p}} \times \ddot{\boldsymbol{p}}. \tag{139}$$

We denote the coordinates of the dipole moment in the frame corotating with the grain with unprimed indices, and the ones in the 'lab frame' with primed indices. Take a grain rotating around the z-axis, without precession, with angular frequency ω. We have

$$\begin{aligned} p_x' &= \cos\omega t p_x - \sin\omega t p_y, \\ p_y' &= \sin\omega t p_x + \cos\omega t p_y \quad \text{and} \\ p_z' &= p_z. \end{aligned} \tag{140}$$

A straightforward calculation leads to the following expressions in the lab frame:

$$\begin{aligned} \ddot{\boldsymbol{p}}^2 = {} & \ddot{p}_x^2 + \ddot{p}_y^2 + \ddot{p}_z^2 + 4\omega\left(\dot{p}_x\ddot{p}_y - \dot{p}_y\ddot{p}_x\right) \\ & + \omega^2\left[4\left(\dot{p}_x^2 + \dot{p}_y^2\right) - 2\left(p_x\ddot{p}_x + p_y\ddot{p}_y\right)\right] \\ & + 4\omega^3\left(p_x\dot{p}_y - p_y\dot{p}_x\right) + \omega^4\left(p_x^2 + p_y^2\right) \end{aligned} \tag{141}$$

and

$$\begin{aligned} (\dot{\boldsymbol{p}} \times \ddot{\boldsymbol{p}})_z = {} & \dot{p}_x\ddot{p}_y - \dot{p}_y\ddot{p}_x + \omega\left[2\left(\dot{p}_x^2 + \dot{p}_y^2\right) - \left(p_x\ddot{p}_x + p_y\ddot{p}_y\right)\right] \\ & + 3\omega^2\left(p_x\dot{p}_y - p_y\dot{p}_x\right) + \omega^3\left(p_x^2 + p_y^2\right). \end{aligned} \tag{142}$$

Since we are interested in the statistical properties of the emission, we define the unequal-time dipole moment correlation function in grain coordinates,

$$C_{ij}(\tau) \equiv \left\langle (p_i(t) - \langle p_i\rangle)(p_j(t+\tau) - \langle p_j\rangle)\right\rangle, \tag{143}$$

where $\langle p_i\rangle = \mu_i$ is just the constant dipole moment of the grain. We further assume statistical spherical symmetry of the dipole moment in the grain coordinates, i.e. $C_{ij} = C\delta_{ij}$. (For a planar grain, the values of the correlation functions depend on the in-plane or out-of-plane character of the vibrational modes and may be anisotropic. However, if the infrared emission arises during thermal spikes when the grain is not rotating around its axis of greatest angular momentum, we expect the isotropic analysis to be a good approximation.) The average values of the previous formulae then become[10]

$$\langle\ddot{\boldsymbol{p}}^2\rangle = 3C''''(0) - 12\omega^2 C''(0) + 2\omega^4 C(0) \tag{144}$$

and

$$\langle\dot{\boldsymbol{p}} \times \ddot{\boldsymbol{p}}\rangle_z = -6\omega C''(0) + 2\omega^3 C(0), \tag{145}$$

where $'$ denotes the derivative of the correlation function with respect to τ.

The Wiener–Khintchine theorem relates the correlation functions to the spectral density S_ν, $C(\tau) = \int_0^\infty S_\nu \cos(2\pi\nu\tau)\mathrm{d}\nu$. Plugging back into equations (144) and (145), we get

$$\langle\ddot{\boldsymbol{p}}^2\rangle = \int_0^\infty \left[3(2\pi\nu)^4 + 12\omega^2(2\pi\nu)^2 + 2\omega^4\right] S_\nu \,\mathrm{d}\nu \tag{146}$$

and

$$\langle\dot{\boldsymbol{p}} \times \ddot{\boldsymbol{p}}\rangle_z = \int_0^\infty \left[6\omega(2\pi\nu)^2 + 2\omega^3\right] S_\nu \,\mathrm{d}\nu. \tag{147}$$

Now making use of the assumption that the grain rotates slowly, i.e. that $\nu_{\rm rot} \equiv \omega/2\pi \ll \nu_0 \equiv$ typical frequency of emission, in the infrared, we get, at the lowest order in $\nu_{\rm rot}/\nu_0$, the average total power and average total rate of radiation of angular momentum:

$$\left\langle \frac{\mathrm{d}E}{\mathrm{d}t} \right\rangle = \frac{2}{3c^3}\langle\ddot{\boldsymbol{p}}^2\rangle = \frac{2}{c^3}\int_0^\infty (2\pi\nu)^4 S_\nu \,\mathrm{d}\nu \tag{148}$$

and

$$\left\langle \frac{\mathrm{d}L_z}{\mathrm{d}t} \right\rangle = \frac{2}{3c^3}\langle\dot{\boldsymbol{p}} \times \ddot{\boldsymbol{p}}\rangle_z = \frac{4\omega}{c^3}\int_0^\infty (2\pi\nu)^2 S_\nu \,\mathrm{d}\nu. \tag{149}$$

If one knows the infrared power radiated per steradian per frequency interval F_ν, such that

$$\left\langle \frac{\mathrm{d}E}{\mathrm{d}t} \right\rangle = 4\pi\int_0^\infty F_\nu \,\mathrm{d}\nu, \tag{150}$$

one can deduce the rate of angular momentum loss through infrared emission:

$$\left\langle \frac{\mathrm{d}L_z}{\mathrm{d}t} \right\rangle = \frac{2\omega}{\pi}\int_0^\infty \frac{F_\nu}{\nu^2}\,\mathrm{d}\nu. \tag{151}$$

This result is twice as big as the one given in DL98b. [The difference occurs because DL98b modelled the dipole fluctuations with six uncorrelated rotating dipoles, one rotating each direction in the xy, yz and xz planes. They counted the radiated power from all six of these, but only considered the angular momentum loss from two of them (in the xy plane). The dipoles rotating in the xz and yz planes containing the rotation axis also emit net angular momentum however, and if they are considered one recovers the factor of 2.]

This classical treatment does not predict the rotational excitation from the recoil given by individual photons, which is a quantum effect. As in DL98b, we set

$$\left\langle \frac{\mathrm{d}\Delta L^2}{\mathrm{d}t} \right\rangle = \frac{\mathrm{d}N_{\rm phot}}{\mathrm{d}t}\hbar^2 = \frac{h}{\pi}\int_0^\infty \frac{F_\nu}{\nu}\,\mathrm{d}\nu. \tag{152}$$

The normalized damping and excitation rates are then

$$\begin{aligned} F_{\rm IR} &= \frac{2\tau_{\rm H}}{\pi I}\int_0^\infty \frac{F_\nu}{\nu^2}\,\mathrm{d}\nu \text{and} \\ G_{\rm IR} &= \frac{h}{6\pi I}\frac{\tau_{\rm H}}{kT}\int_0^\infty \frac{F_\nu}{\nu}\,\mathrm{d}\nu. \end{aligned} \tag{153}$$

We calculate the infrared emissivity of PAHs and small carbonaceous grains using the 'thermal continuous' approximation, described in DL01. They indeed show that this treatment leads to spectra very close to those predicted by the exact statistical treatment, and has the advantage of being computationally much faster. We obtain the steady-state energy distribution function and then get the infrared emissivity, as explained in DL01.

We checked numerically that we recover DL98 result for low values of the radiation field intensity: $F_{\rm IR}, G_{\rm IR} \propto \chi$. However, their result for high values of the radiation field ($F_{\rm IR} \propto \chi^{2/3}$, $G_{\rm IR} \propto \chi^{5/6}$) relies on the fact that the absorption efficiency $Q_\nu \propto \nu^2$ at the characteristic frequencies of infrared emission. This is not valid anymore for high-radiation fields, which offset the emission spectrum to higher frequencies, where the absorption efficiency has not a simple dependence on frequency anymore. We show the resulting infrared emission damping and excitation coefficients in Fig. 7.

8 PHOTOELECTRIC EMISSION

An electron ejected from the grain carries away an angular momentum along the rotation axis (z-axis) equal to:

$$\Delta L_z = m_e\rho\left(v_\phi' - \rho\omega\right), \tag{154}$$

[10] Expectation values of derivatives such as $\langle\dot{p}_x^2\rangle$ can be expressed in terms of correlation functions via integration by parts. In this case, $\langle\dot{p}_x^2\rangle = \langle(p_x\dot{p}_x)'\rangle - \langle p_x\ddot{p}_x\rangle$. The first term vanishes for a stationary process, and the second is $-C'(0)$.

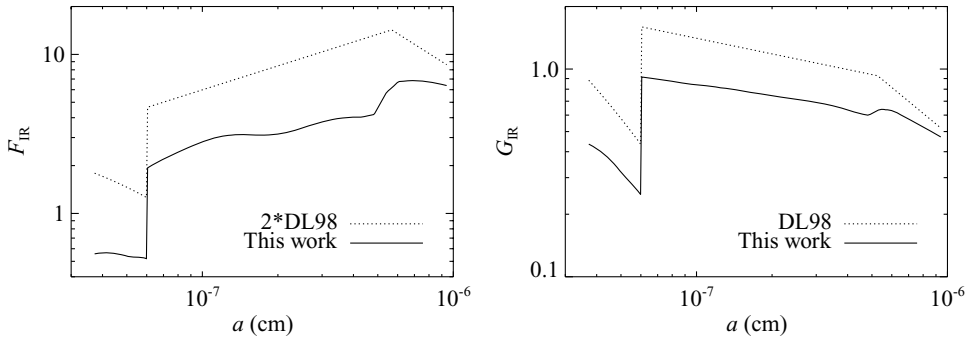

Figure 7. Infrared emission damping and excitation coefficients F_{IR} and G_{IR} in CNM conditions (equation 162), compared with DL98b result. The difference is mainly due to differences in grain absorption efficiencies and the calculation of the infrared spectrum. We used Li & Draine (2001b) absorption efficiencies and DL01 model to compute the infrared emissivity. The kink at 50 Å in our result is due to a change in optical properties of dust grains. The kink around 50 Å in DL98b result is due to the change from constant temperature limit (larger grains) to thermal spikes limit (smaller grains). The fact that they coincide is purely chance, and would not be necessarily the case for other environmental conditions. The discontinuity at 6 Å is due to the change in grain shape.

where v'_ϕ is its tangential velocity in the grain frame. From this, we deduce that

$$F_{\rm pe} = \frac{m_{\rm e}}{m_{\rm H}} \frac{J_{\rm pe}}{2\pi a_{\rm s}^2 n_{\rm H} \sqrt{2kT/\pi m_{\rm H}}}, \tag{155}$$

where $J_{\rm pe}$ is the photoemission rate and was described in Section 3.4. The excitation rate can be obtained by first noticing that the rotational velocity is much smaller than the velocity of ejected electrons:

$$a\omega \ll v'_\phi \tag{156}$$

so that we have, up to small corrections

$$\Delta L_z^2 = m_{\rm e}^2 \rho^2 v_\phi'^2. \tag{157}$$

We assume a cosine-law directional distribution for escaping electrons, so that $\langle v_\phi'^2 \rangle = \frac{1}{4} v_{\rm e}^2$, where we denote $v_{\rm e}$ the average velocity of the electron at the grain surface. The latter satisfies

$$\frac{1}{2} m_{\rm e} v_{\rm e}^2 - \frac{(Z_{\rm g}+1) q_{\rm e}^2}{a_{\rm s}} = E_{\rm pe}, \tag{158}$$

where $E_{\rm pe}$ is the average energy at infinity of the photoejected electron. We finally get

$$\langle \Delta L_z^2 \rangle = m_{\rm e}^2 \frac{2}{3} \frac{a_{\rm cx}^4}{a_{\rm s}^2} \frac{1}{4} v_{\rm e}^2 = \frac{m_{\rm e}}{3} \frac{a_{\rm cx}^4}{a_{\rm s}^2} \left[E_{\rm pe} + \frac{(Z_{\rm g}+1) q_{\rm e}^2}{a_{\rm s}} \right]. \tag{159}$$

So the normalized excitation rate is

$$G_{\rm pe} = \frac{m_{\rm e}}{4 n_{\rm H} (8\pi m_{\rm H} kT)^{1/2} a_{\rm s}^2 kT} \left[\Gamma_{\rm pe} + \frac{(Z_{\rm g}+1) q_{\rm e}^2}{a_{\rm s}} J_{\rm pe} \right], \tag{160}$$

where $\Gamma_{\rm pe}$ is the heating rate due to photoemission of electrons, obtained from WD01b.

9 RANDOM H_2 FORMATION

DL98b showed that the random formation of H_2 molecules on the grain surface does not make a major contribution to rotational excitation. We use their result,

$$G_{\rm H_2} = \frac{\gamma}{4}(1-y) \frac{E_f}{kT} \left[1 + \frac{\langle J(J+1) \rangle \hbar^2}{2 m_{\rm H} E_f a_x^2} \right], \tag{161}$$

where γ is the efficiency of H_2 formation, $y = 2n_{\rm H_2}/n_{\rm H}$, $E_f \approx 0.2$ eV is the average translational kinetic energy of the nascent H_2, and $\langle J(J+1) \rangle \approx 10^2$ gives its average angular momentum.

10 RESULTING EMISSIVITY AND EFFECT OF VARIOUS PARAMETERS

Throughout this section, and unless otherwise stated, we will take as a fiducial environment the CNM parameters specified by

$$\begin{aligned} &n_{\rm H} = 30\,{\rm cm}^{-3},\ T = 100\,{\rm K} \\ &x_{\rm H} \equiv n({\rm H}^+)/n_{\rm H} = 10^{-3}, \quad x_{\rm C} \equiv n({\rm C}^+)/n_{\rm H} = 3 \times 10^{-4} \\ &\chi \equiv u/u_{\rm ISRF} = 1, \quad \gamma = 0. \end{aligned} \tag{162}$$

We also take the rms intrinsic dipole moment to be

$$\langle \mu_{\rm i}^2 \rangle^{1/2} \left(a = 10^{-7} {\rm cm} \right) = 9.3\,{\rm debye}. \tag{163}$$

For the size distribution parameters, we use those given by WD01a for a ratio of visual extinction to reddening $R_V = 3.1$, and a carbon abundance in the log-normal distributions $b_C = 6 \times 10^{-5}$.

This section is intended to give some intuition into the effect of various parameters on the spinning dust spectrum. However, the reader should keep in mind that environmental parameter space is many-dimensional, and changing several parameters at once may lead to modifications that are not superpositions of the effects described here.

10.1 General shape of the rotational distribution function

The rotational distribution function is obtained as described in Section 4. We remind the reader that the Fokker–Planck equation is not stricltly valid for the smallest grains, for which impulsive torques are important. It however still describes their rotational distribution function with more accuracy than a simple Maxwellian. Moreover, DL98 showed that the impulsive torques may be neglected for grain radii $a \geq 7$ Å. In Fig. 8, we show that the rotational distribution function obtained by the Fokker–Planck equation differs significantly from a Maxwellian. It has a sharper cut-off at high frequencies due to the proper accounting for rotational damping through electric dipole radiation.

In what follows, we will analyse the effect of various parameters on the spinning dust emissivity. As can be seen from equation (33) and the expressions derived next for the normalized damping and excitation rates, the rotational distribution function has complex dependencies on all grain and environmental parameters. To get some intuition on the physics of spinning dust and the influence of each parameter, we will rely on a simplified expression for the

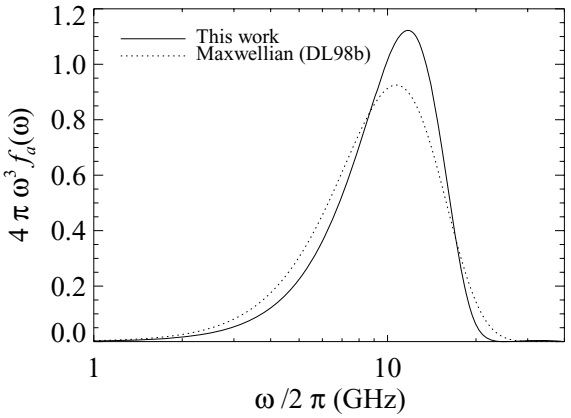

Figure 8. Rotational distribution function for a grain radius $a = 7$ Å in CNM conditions, for a single value of the dipole moment $\mu_{\rm i}(10^{-7}\,{\rm cm}) = 9.3$ debye. The plot compares the solution of the Fokker–Planck equation with the DL98b Maxwellian approximation (DL98b equation 57 used with our F, G). Note that DL98b prescription gives $(\langle\omega^2\rangle)^{1/2} = 2\,\pi \times 10.7$ GHz, which is in excellent agreement with the value we get, $(\langle\omega^2\rangle)^{1/2} = 2\,\pi \times 10.9$ GHz. However, the shape of the distribution function is significantly different.

rotational distribution function in the following sections:

$$f_{\rm a}(\omega) \propto \exp\left[-\frac{F}{G}\frac{I\omega^2}{2kT} - \frac{\tau_{\rm H}}{3G\tau_{\rm ed}}\left(\frac{I\omega^2}{2kT}\right)^2\right], \tag{164}$$

where we approximate the plasma drag excitation rate (which is in principle a function of ω) by the constant

$$G_{\rm p} \approx G_{\rm p}(\omega_{\rm th})\,,\ \omega_{\rm th} \equiv \left(\frac{3kT}{I}\right)^{1/2}. \tag{165}$$

In our analysis we will also neglect the charge-displacement induced dipole moment as it has a minor contribution. Of course, the actual rotational distribution function and emissivity are computed using the exact equations developed in this paper.

For a given grain radius a and intrinsic electric dipole moment $\mu_{\rm i}$, the power radiated is $P_\nu(a;\mu_{\rm i}) \propto \nu^6 f_{\rm a}(2\pi\nu;\mu_{\rm i})$. It is straightforward, from equation (164), to show that the peak frequency is given by

$$\nu_{\rm peak} \approx \left(\frac{2}{1+\sqrt{1+\xi}}\frac{G}{F}\right)^{1/2}\frac{1}{2\pi}\sqrt{\frac{6kT}{I}}, \tag{166}$$

where we defined the parameter

$$\xi \equiv \frac{8G}{F^2}\frac{\tau_{\rm H}}{\tau_{\rm ed}} \tag{167}$$

which denotes the non-Maxwellian character of the distribution function.

For $\xi \ll 1$, the distribution is nearly Maxwellian,

$$f_{\rm a}(\omega) \propto \exp\left(-\frac{F}{G}\frac{I\omega^2}{2kT}\right), \tag{168}$$

and the peak frequency is given by

$$\nu_{\rm peak} \approx \left(\frac{G}{F}\right)^{1/2}\frac{1}{2\pi}\sqrt{\frac{6kT}{I}}\ (\xi \ll 1). \tag{169}$$

Moreover, the total power emitted by a single grain $j_{\rm a} \propto \mu^2 \int \omega^6 f_{\rm a}(\omega){\rm d}\omega$ has the following dependence:

$$j_{\rm a} \propto \mu^2\left(\frac{G}{F}\right)^2 T^2\ (\xi \ll 1). \tag{170}$$

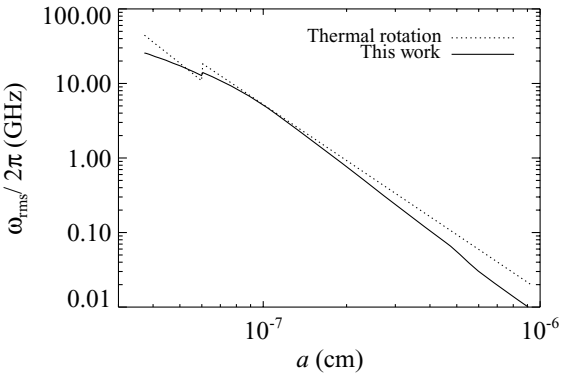

Figure 9. rms rotation rate $\omega_{\rm rms} \equiv \langle\omega^2\rangle^{1/2}$ as a function of grain radius a, for CNM conditions. The rotation rate the grain would achieve if it were rotating thermally (in that case $\omega_{\rm rms} = \sqrt{3kT/I}$) is also shown. It can be seen that the grains rotate subthermally. The kink at 6 Å is due to the change in grain geometry.

For $\xi \gg 1$, the distribution is strongly non-Maxwellian,[11]

$$f_{\rm a}(\omega) \propto \exp\left[-\frac{\tau_{\rm H}}{3G\tau_{\rm ed}}\left(\frac{I\omega^2}{2kT}\right)^2\right], \tag{171}$$

and the peak frequency is given by

$$\nu_{\rm peak} \approx \left(\frac{G\tau_{\rm ed}}{2\tau_{\rm H}}\right)^{1/4}\frac{1}{2\pi}\sqrt{\frac{6kT}{I}}\ (\xi \gg 1). \tag{172}$$

The total power is then given by

$$j_{\rm a} \propto \mu^2\frac{G\tau_{\rm ed}}{\tau_{\rm H}}T^2\ (\xi \gg 1). \tag{173}$$

In Fig. 9, we show the rms rotation rate $\langle\omega^2\rangle^{1/2}$ as a function of grain radius. As can be expected, the smallest grains are rotating with the greatest angular velocity, as they have the smallest moment of inertia. Consequently, they radiate at the highest frequencies, and constitute the peak of the spectrum. Therefore, we will use equations (164) to (173) for a grain of radius $a_{\rm min} = 3.5$ Å to evaluate the effect of various parameters on the emissivity.

We finally remind the reader with the dependencies of characteristic time-scales :

$$\tau_{\rm H} \propto n_{\rm H}^{-1}T^{-1/2},\quad \tau_{\rm ed} \propto \mu^{-2}T^{-1}. \tag{174}$$

10.2 Emissivity

Once the rotational distribution function is known, as a function of the intrinsic electric dipole moment, $f_{\rm a}(\omega\,;\,\mu_{\rm i})$, one can get the power radiated by a grain of radius a by averaging over the intrinsic dipole moments Gaussian distribution $P(\mu_{\rm i})$ defined in equation (8). One gets

$$P_\nu(a) = \int {\rm d}\mu_{\rm i} P(\mu_{\rm i})\frac{2}{3}\frac{\mu_\perp^2\omega^6}{c^3}2\pi f_{\rm a}(\omega;\mu_{\rm i}), \tag{175}$$

where $\mu_\perp^2 = \frac{2}{3}\mu^2$ for spherical grains and $\mu_\perp^2 = \mu^2$ for cylindrical grains.

The overall effect of averaging over the dipole moments distribution is to broaden the spectrum, as can be seen in Fig. 10. The peak frequency remains approximately equal to that of $P_\nu(\mu_{\rm i} = \langle\mu_{\rm i}^2\rangle^{1/2})$.

[11] Interestingly, Erickson (1957) had already obtained a result similar to equation (171) with a Fokker–Planck equation.

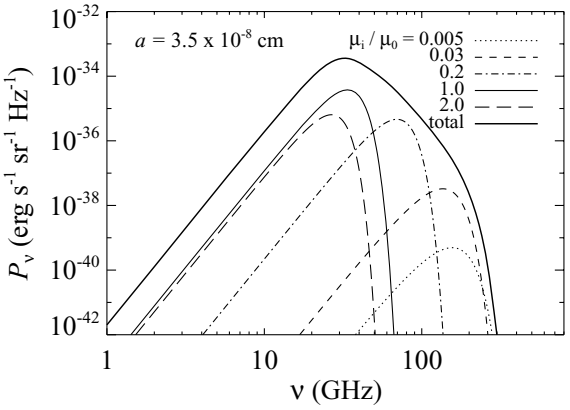

Figure 10. Power radiated by one grain of radius $a = 3.5$ Å in CNM conditions. The dotted and dashed lines show the contributions of various values of the intrinsic dipole moment, which is assumed to have a Gaussian distribution with rms value $\mu_0 \equiv \langle \mu_i^2 \rangle^{1/2}$ (a). The solid line is the total power.

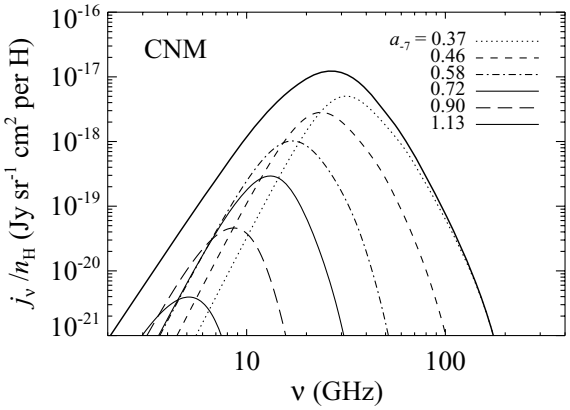

Figure 11. Spinning dust emissivity for CNM environment. Contributions from grains of various sizes are shown [$a_{-7} \equiv a/(10^{-7}\,\mathrm{cm})$]. The grain size distribution parameters are taken from WD01a with $R_V = 3.1$ and $b_c = 6 \times 10^{-5}$.

We will discuss the effect of the rms intrinsic dipole moment in Section 10.3.

The emissivity per H atom is then obtained by integrating the power radiated by each grain over the grain size distribution function, described in Section 3.2. The emissivity for the CNM environment is shown in Fig. 11. Note that the grain size distribution directly weights the spectrum, and thus needs to be known with accuracy, which is not quite the case yet for the very small grains.

10.3 Effect of the rms intrinsic dipole moment $\langle \mu_i^2 \rangle^{1/2}$

Varying the rms intrinsic dipole moment affects the spectrum in three main ways. First, it affects the total power radiated, as $P_\nu \propto \mu^2$. Then, it affects the non-Maxwellian character of the distribution function, as $\tau_{ed} \propto \mu^2$. Finally, it affects the rotational damping and excitation rates essentially through plasma drag, which has $G_p \propto \mu^2$ (the effect on G_i is not as important).

Throughout the range of values considered

$$1\,\mathrm{debye} < \mu_i(10^{-7}\,\mathrm{cm}) < 100\,\mathrm{debye}, \tag{176}$$

and in CNM conditions, the distribution function remains strongly non-Maxwellian : $\xi \gtrsim 60$. Therefore, we can use the strongly non-Maxwellian limit equation (172) to evaluate the peak frequency.

Low dipole moment limit. For low values of the electric dipole moment, plasma drag has little effect on both the rotational damping and excitation. Therefore, F and G are roughly independent of μ, and, from equations (172), (173) and $\tau_{ed} \propto \mu^2$, we get

$$\nu_{peak}\,(\mu_i \to 0) \propto \mu_i^{-1/2} \tag{177}$$

and

$$j/n_H\,(\mu_i \to 0) \to \text{constant}. \tag{178}$$

One can see in Fig. 12 that equation (177) is quite accurately satisfied. The total power has a weak dependence on μ_i for low values of the intrinsic dipole moment, but is not strictly independent of it, which comes from the multiple approximations made in this analysis (neglecting the charge displacement-induced dipole moment, and using equation (173) for the total power, after integration over the size distribution, instead of the total power radiated by a single grain).

High dipole moment limit. For high values of the electric dipole moment, plasma drag dominates both rotational damping and excitation. Therefore, $G \approx G_p \propto \mu^2$ and so we get

$$\nu_{peak}\,(\mu_i \to \infty) \to \text{constant} \tag{179}$$

and

$$j/n_H\,(\mu_i \to \infty) \propto \mu_i^2 \tag{180}$$

which describe approximately the behaviour observed in Fig. 12.

10.4 Effect of the number density n_H

The main effects of the number density are:

(i) Changing the relative contribution of gas-induced and radiation-induced rotational damping and excitation. For very low number densities, F_{IR} and $G_{IR} \propto \tau_H \propto n_H^{-1}$ dominate over other

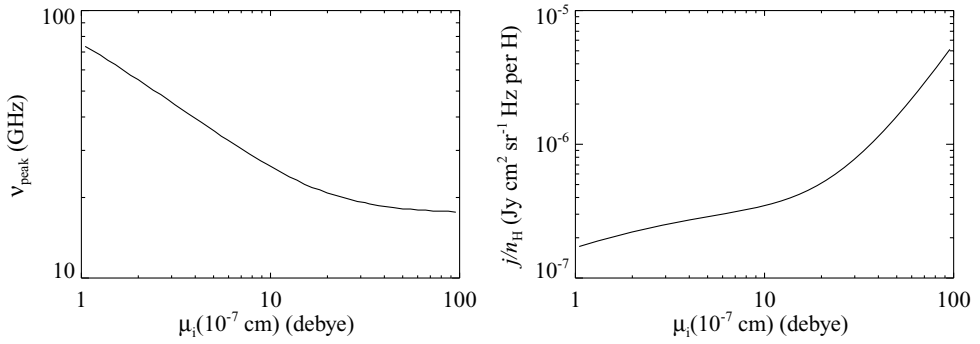

Figure 12. Effect of the intrinsic electric dipole moment on the peak frequency and the total spinning dust emission. Environmental parameters are set to CNM conditions defined in equation (162). Increasing the electric dipole moment decreases the peak frequency and increases the total power radiated.

rotational damping and excitation rates. For high densities, plasma drag and collisions are dominant. Note that the charge distribution is also modified as the density is higher, the more important is collisional charging compared to photoemission. As a consequence, the grains are positively charged at low densities, and tend to be negatively charged at high densities, due to the higher rate of collisions with electrons.

(ii) Influencing the non-Maxwellian character of the rotational distribution function. The higher the number density, the closer is the distribution function to a Maxwellian. Numerical calculation shows that starting from CNM conditions and varying only $n_{\rm H}$, we transition to the Maxwellian regime ($\xi \lesssim 1$) if $n_{\rm H} \gtrsim 10^5\,{\rm cm}^{-3}$.

Low-density limit. For very low number densities, the distribution is highly non-Maxwellian and we can use equations (172) and (173), with $G = G_{\rm IR}$, to estimate the peak frequency and total power. As $G_{\rm IR}/\tau_{\rm H}$ is independent of $n_{\rm H}$, both the number density and total power should asymptote to a constant value. We can estimate numerically the peak frequency in CNM conditions and get

$$\nu_{\rm peak}\,(n_{\rm H} \to 0) \approx 13\,{\rm GHz} \tag{181}$$

and

$$j/n_{\rm H}\,(n_{\rm H} \to 0) \to \text{constant}, \tag{182}$$

which is in good agreement with Fig. 13.

Intermediate densities. Over the range $10^2\,{\rm cm}^{-3} \lesssim n_{\rm H} \lesssim 10^4\,{\rm cm}^{-3}$, gas processes are dominant over infrared emission, so F and G are roughly independent of $n_{\rm H}$. In addition, the distribution is still strongly non-Maxwellian. Using equations (172) and (173), we thus find

$$\nu_{\rm peak}\left(10^2\,{\rm cm}^{-3} \lesssim n_{\rm H} \lesssim 10^4\,{\rm cm}^{-3}\right) \propto n_{\rm H}^{1/4} \tag{183}$$

and

$$j/n_{\rm H}\left(10^2\,{\rm cm}^{-3} \lesssim n_{\rm H} \lesssim 10^4\,{\rm cm}^{-3}\right) \propto n_{\rm H}. \tag{184}$$

The kink around $n_{\rm H} \sim 3 \times 10^3\,{\rm cm}^3$ is due to our discontinuous treatment of the evaporation temperature for high densities (see Section 5.1.4), and to the replacement of the integration over all grain radii by a discrete summation when numerically computing the spectrum. Therefore, the spectra should not be considered as very accurate in that region.

High-density limit. For very high number densities, the excitation and damping is dominated by gas processes, and the electric dipole damping becomes negligibly small, so that the rotational distribution function is actually a Maxwellian, although not thermal. Using equations (169) and (170), we find

$$\nu_{\rm peak}\,(n_{\rm H} \to \infty) \approx 150\,{\rm GHz} \tag{185}$$

and

$$j/n_{\rm H}\,(n_{\rm H} \to \infty) \to \text{constant}. \tag{186}$$

10.5 Effect of the gas temperature T

Temperature has a less obvious effect on the spectrum and we need to analyse in detail every damping and excitation process. It turns out that the charge distribution of the smallest grains varies very little over the range of temperature considered $1 < T < 10^5$ K and they remain mostly neutral throughout this interval. The distribution remains strongly non-Maxwellian for T greater than a few K.

Low-temperature limit. At very low temperatures, the dominant excitation process is collisions with ions. Indeed, the grains being mostly neutral, the ions interact strongly with the electric dipole potential. As $\tilde{\mu} \propto T^{-1}$ and $\phi \propto T^{-1/2}$, one can see from equations (102) and (104) that $G_{\rm i} \propto T^{-2}$. Plasma drag has also $G_{\rm p} \propto T^{-2}$ in principle, but this becomes a shallower power law at low temperatures as the interaction time-scale becomes longer than the rotation time-scale. We find numerically, though, that roughly $G \propto T^{-1.5}$ as G is not strictly equal to $G_{\rm i}$ (collisions with neutrals are also significant at low temperatures). Using equations (169), (170) and (174), we find

$$\nu_{\rm peak}\left(3{\rm K} \lesssim T \lesssim 10^2{\rm K}\right) \approx 35\,{\rm GHz} \tag{187}$$

and

$$j/n_{\rm H}\left(3{\rm K} \lesssim T \lesssim 10^2\,{\rm K}\right) \approx \text{constant}. \tag{188}$$

Note that for extremely low temperatures, the distribution would become Maxwellian, and one would get, according to equations (172), (173),

$$\nu_{\rm peak}\,(T \to 0) \propto T^{1/2} \tag{189}$$

and

$$j/n_{\rm H}\,(T \to 0) \propto T^2 \tag{190}$$

which can be guessed at the extreme low temperature end of Fig. 13. Temperatures below ∼3 K are of course unphysical, but for other environmental conditions than those of equation (162), the behaviour discussed above could take place at higher, observed temperatures.

High-temperature limit. At very high temperatures, collisions with neutrals are the dominant damping and excitation process. The CNM environment being mostly neutral, $F_{\rm n} \to 1$ and $G_{\rm n} \to 1/2$ at high temperatures [$G_{\rm n}^{(\rm ev)} \propto T_{\rm ev}/T \to 0$]. Moreover, the distribution becomes strongly non-Maxwellian, as $\xi \propto T^{1/2}$. We therefore obtain

$$\nu_{\rm peak}(T \to \infty) \approx 200 T_5^{3/8}{\rm GHz} \tag{191}$$

and

$$j/n_{\rm H}\,(T \to \infty) \propto T^{3/2}. \tag{192}$$

Fig. 13 shows that these power laws describe the behaviour of the peak frequency and total power with very good accuracy.

10.6 Effect of the radiation field intensity χ

The radiation field affects the spectrum through only two ways. First of all, it changes the charge distribution of the grains as an increased radiation implies a higher photoemission rate. Second of all, it affects the rate of damping and excitation through infrared emission (and photoelectric emission, but this is subdominant).

Low-radiation intensity limit. In a low-radiation field, $F_{\rm rad}$ and $G_{\rm rad}$ become negligible. The photoemission charging rate becomes insignificant compared with collisional charging, and the charge distribution function depends only on other environmental parameters. Thus, one expects the spectrum to reach an asymptotic shape for very low-radiation fields. The distribution is strongly non-Maxwellian, and the dominant excitation mechanism is collisions with ions, whereas the dominant damping mechanisms are plasma drag and collisions with neutrals. Thus, we find

$$\nu_{\rm peak}(\chi \to 0) \approx 35\,{\rm GHz} \tag{193}$$

and

$$j/n_{\rm H}\,(\chi \to 0) \to \text{constant}. \tag{194}$$

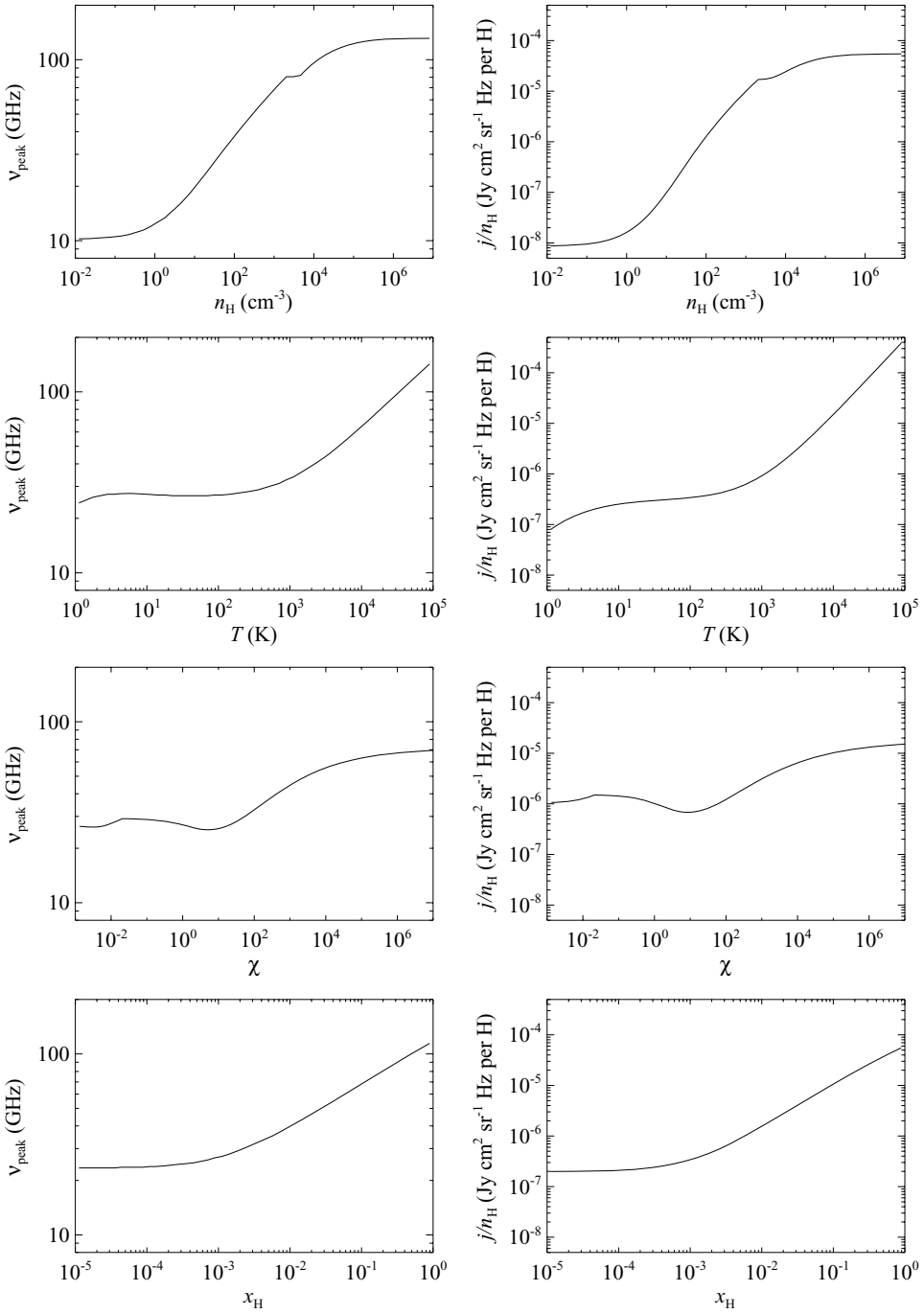

Figure 13. Effect of various environmental parameters on the peak frequency and the total spinning dust emission. When one parameter is varied, other environmental parameters are set to CNM conditions defined in equation (162). See Sections 10.4 to 10.7 for a detailed description.

The kink around $\chi \sim 2 \times 10^{-2}$ is due to our discontinuous treatment of the evaporation temperature for low intensities of the radiation field.

Around $\chi \approx 1$–10, the grain becoming more and more positively charged, the collisions with ions start being less efficient, although still the dominant excitation mechanism. This results in a slight decrease in both ν_{peak} and j/n_H.

High-radiation intensity limit. In a high-radiation field, $F \approx F_{IR}$ and $G \approx G_{IR}$. Both F_{IR} and G_{IR} are approximately (although not strictly) linear in χ, as shown in DL98b for the thermal spikes limit (see their equations 31 and 44). Thus, $\xi \sim \chi^{-1}$, so the distribution becomes Maxwellian. The peak frequency and total emitted power are then given by equations (169) and (170), which imply that

$$\nu_{peak}(\chi \to \infty) \approx \text{constant} \tag{195}$$

and

$$j/n_H(\chi \to \infty) \approx \text{constant}. \tag{196}$$

These asymptotic forms are not strictly valid because F_{IR} and G_{IR} are not strictly linear in χ, and do not have a simple dependence on that parameter.

10.7 Effect of the ionization fraction x_H

The hydrogen ionization fraction affects the charge distribution by modifying the contribution from collisions with protons. It also changes the contribution of collisions with ions, neutrals and plasma drag. Characteristic time-scales are left invariant, and $\xi \gg 1$ for any ionization fraction in otherwise CNM conditions.

Low-ionization fraction limit. In that limit, the rotational distribution function reaches an asymptotic form where collisions with protons and plasma drag due to protons can be neglected. However, there are still C^+ ions in the gas, so collisions with ions and plasma drag may still be important, although the dominant excitation process is collisions with neutrals. We find

$$\nu_{\rm peak}\,(x_{\rm H} \to 0) \approx 30\,{\rm GHz} \tag{197}$$

and

$$j/n_{\rm H}\,(x_{\rm H} \to 0) \to \text{constant}. \tag{198}$$

High-ionization fraction limit. In that case, collisions with ions are the dominant excitation process. Using equations (172) and (173) along with $G \approx G_{\rm i} \propto x_{\rm H}$, we find

$$\nu_{\rm peak}(x_{\rm H} \to 1) \approx 90(x_{\rm H}/0.1)^{1/4}\,{\rm GHz} \tag{199}$$

and

$$j/n_{\rm H}\,(x_{\rm H} \to 1) \propto x_{\rm H}. \tag{200}$$

10.8 Concluding remarks

We remind the reader that all the estimates in the previous section were given by assuming that the peak frequency of the spinning dust spectrum is determined by that of the smallest grains, and that the total power follows the same dependence upon environmental parameters as the power emitted by the smallest grains. Therefore, they should be taken as an aid to understand the physics of spinning dust, but not as an accurate description, which requires numerical calculations.

The overall conclusion of this section is that varying a single environmental parameter may change the peak frequency by up to an order of magnitude, and the total emitted power by several orders of magnitude. There is therefore a very large range of possible peak frequencies and total powers that can be produced by spinning dust radiation. Multiphase environments, in particular, could emit very broad spinning dust spectra. Deducing the environmental parameters from an observed spectrum could therefore be a difficult task.

We show the spinning dust spectrum for various environments and compare them to DL98 results in Fig. 14.

11 CONCLUSION

We have presented a detailed analysis of the rotational excitation and damping of small carbonaceous grains. We have refined DL98b

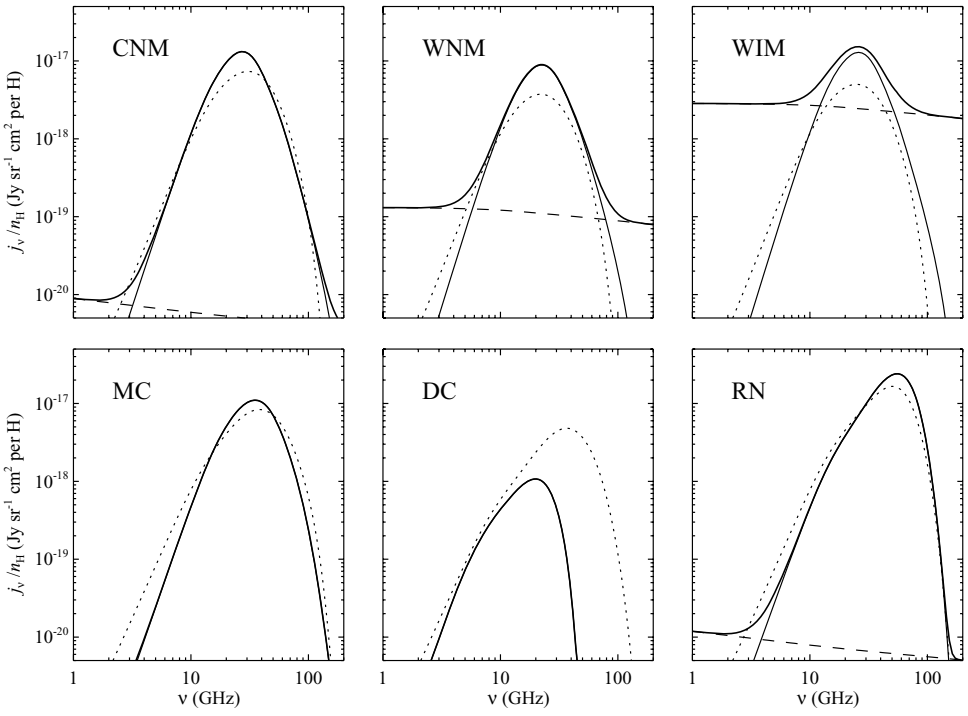

Figure 14. Spinning dust spectra for several environmental conditions: cold neutral medium (CNM), warm neutral medium (WNM), warm ionized medium (WIM), molecular cloud (MC), dark cloud (DC) and reflection nebula (RN). The environments are defined in DL98b, table 1. The thin solid line is the result of our calculation, the dotted line being DL98 prediction (obtained from B. T. Draine's website: http://astro.princeton/∼draine) and the dashed line is the free–free emission (the free–free gaunt factor were taken from Sutherland 1998). The parameters for the grain size distribution are: $R_V = 3.1$, $b_C = 6 \times 10^{-5}$ for the diffuse CNM, WNM and WIM environments, and $R_V = 5.5$, $b_C = 3 \times 10^{-5}$ for the dense MC, DC and RN environments. The apparent systematic increase of power around the peak frequency for our result is mainly due to the grain size distribution we use, which has an increased number of small grains compared to that used by DL98 (compare e.g. fig. 2 from WD01a with fig. 8 from DL98b). Note that for the DC environment, for which rotational excitation and damping is dominated by collisions with neutral species (mainly H_2 molecules), DL98 prediction largely overestimates the peak frequency and total power because they underestimate the damping rate (see equation 53 and subsequent discussion).

results in the case of collisions, accounting properly for the centrifugal potential which increases the net damping rate. In the case of collisions with ions, we accounted for the effect of the electric dipole potential on the collision cross-section. We found that this is a small effect in the case of charged grains, but that it may significantly increase the damping and excitation rates in the case of neutral grains. We evaluated the contribution of 'plasma drag' by considering hyperbolic trajectories and rotating grains in the case of charged grains, and straight lines in the case of neutral grains. We corrected DL98b results for the damping through infrared emission. Finally, we calculated the rotational distribution function by solving the Fokker–Planck equation.

We believe our model provides a much more accurate description of the spinning dust spectrum than previous work. However, we would like to remind the reader of its uncertainties and limitations. First, our model only computes the total intensity of the emitted radiation and not the polarization, which would require an additional study of the alignment mechanisms for PAHs. Secondly, the properties of dust grains are poorly known.

(i) The size distribution and abundance of the smallest grains is uncertain, and in particular the nature of the cut-off at small grain sizes $a \sim a_{\rm min}$ can have a large effect on the spectrum.

(ii) The permanent electric dipole moments of dust grains are not directly constrained by other dust observables. Given that it cannot be computed from first principles, one may regard it as a free parameter (or parameters) of the spinning dust model.

Thirdly, we made some simplified calculations in some cases, as an accurate calculation would have been intractable numerically or substantially complicated the code.

(i) We used the Fokker–Planck approximation, which starts to break down for our smallest grains because a single collision suffices to change the rotational state. We expect that the main consequence of a full treatment would be a tail in the emission spectrum extending to high frequencies, because impulsive collisions would be able to increase the rotation velocities of the grains to $>2\nu_{\rm peak}$ before dissipative forces had time to act (an effect missed by the Fokker–Planck treatment). Therefore, one should not place too much confidence in the many order-of-magnitude falloff at $\sim$100 GHz seen in most of our models. (In many cases this will be unimportant observationally since at high frequencies the vibrational dust contribution is dominant.)

(ii) In the plasma drag calculation, we neglected the electric dipole potential when evaluating the trajectory of ions, taking the straight line (neutral grain) or hyperbolic (charged grain) approximation. Relying on the study of collisions with ions, we may expect the dipole moment to have a small effect in the case of a charged grain. On the other hand, its effect in the case of a neutral grain may be more important, as in that case the electric dipole potential provides the dominant interaction.

(iii) We assumed that the evaporation temperature for the smallest grains was the 'temperature' of the grain just after it has absorbed a UV photon. This is a physically motivated assumption but its validity is not established. The evaporation temperature can have a significant effect on the spectrum, as can be seen from Fig. 3, and one should be aware of the uncertainty in this parameter. Also, we assumed that collisions transition from being sticking to elastic, as the density exceeds a given threshold. Our model is therefore inaccurate in the transition region.

(iv) When calculating the infrared emission spectrum of the grains, we used DL01 'thermal continuous' approximation, which is not very accurate to describe the low-energy part of the spectrum. Whereas these uncertainties are not important if one only wants the spectrum F_ν in the mid-infrared, they may lead to significant errors when calculating the corresponding damping and excitation rates, which are proportional to $\int \nu^{-2} F_\nu {\rm d}\nu$ and $\int \nu^{-1} F_\nu {\rm d}\nu$, respectively.

(v) We ignored systematic torques, although this may not be a major omission for the smallest dust grains.

Despite these uncertainties, we believe that this model is the most complete thus far, and will be a useful tool for comparison to observations and testing the spinning dust hypothesis for anomalous microwave emission in various ISM phases.

ACKNOWLEDGMENTS

We thank G. Dobler, B. Draine, D. Finkbeiner and A. Lazarian for numerous conversations about the physics of grain rotation. YA-H. also thanks T. Readhead and T. Pearson for useful discussions. YA-H. and CMH are supported by the US Department of Energy (DE-FG03-92-ER40701) and the National Science Foundation (AST-0807337). The early phase of this project was funded by the NSF grant AST-0607857. CH is supported by the Alfred P. Sloan Foundation. CD acknowledges support from the US *Planck* project, which is funded by the NASA Science Mission Directorate.

REFERENCES

Abramowitz M., Stegun I., 1972, Handbook of Mathematical Functions. Dover, New York
Anderson N., Watson W. D., 1993, A&A, 270, 477
Banday A. J., Dickinson C., Davies R. D., Davis R. J., Górski K. M., 2003, MNRAS, 345, 897
Bonaldi A., Ricciardi S., Leach S., Stivoli F., Baccigalupi C., de Zotti G., 2007, MNRAS, 382, 1791
Casassus S., Cabrera G. F., Förster F., Pearson T. J., Readhead A. C. S., Dickinson C., 2006, ApJ, 639, 951
Casassus S., Nyman L.-Å., Dickinson C., Pearson T. J., 2007, MNRAS, 382, 1607
Casassus S. et al., 2008, MNRAS, 391, 1075
Davies R. D., Dickinson C., Banday A. J., Jaffe T. R., Górski K. M., Davis R. J., 2006, MNRAS, 370, 1125
Dickinson C. et al., 2004, MNRAS, 353, 732
Dickinson C., Davies R. D., Bronfman L., Casassus S., Davis R. J., Pearson T. J., Readhead A. C. S., Wilkinson P. N., 2007, MNRAS, 379, 297
Dickinson C. et al., 2009, ApJ, 690, 1585
Dobler G., Draine B. T., Finkbeiner D. P. 2008, ApJ, submitted (arXiv:0811.1040)
Draine B. T., Lazarian A., 1998a, ApJ, 494, L19
Draine B. T., Lazarian A., 1998b, ApJ, 508, 157 (DL98b)
Draine B. T., Lazarian A., 1999, ApJ, 512, 740
Draine B. T., Li A., 2001, ApJ, 551, 807 (DL01)
Draine B. T., Sutin B., 1987, ApJ, 320, 803
Eriksen H. K., Jewell J. B., Dickinson C., Banday A. J., Górski K. M., Lawrence C. R., 2008, ApJ, 676, 10
Erickson W. C., 1957, ApJ, 126, 480
Finkbeiner D. P., 2004, ApJ, 614, 186
Ferrara A., Dettmar R.-J., 1994, ApJ, 427, 155
Geyling F. T., Westerman H. R., 1971, Introduction to Orbital Mechanics. Addison-Wesley, Reading, MA
Gold B. et al., 2009, ApJS, 180, 265
Hildebrandt S. R., Rebolo R., Rubiño-Martín J. A., Watson R. A., Gutiérrez C. M., Hoyland R. J., Battistelli E. S., 2007, MNRAS, 382, 594
Hinshaw G. et al., 2009, ApJS, 180, 225
Hoyle F., Wickramasinghe N. C., 1970, Nat., 227, 473

Kuo C. L. et al., 2007, ApJ, 664, 687
Landau L. D., Lifshitz E. M., 1965, Quantum Mechanics. Pergamon Press, Oxford
Leach S. M. et al., 2008, A&A, 491, 597
Leitch E. M., Readhead A. C. S., Pearson T. J., Myers S. T., 1997, ApJ, 486, L23
Li A., Draine B. T., 2001a, ApJ, 550, L213
Li A., Draine B. T., 2001b, ApJ, 554, 778
Marlow W. C., 1965, Proc. Phys. Soc., 86, 731
Mathis J. S., Mezger P. G., Panagia N., 1983, A&A, 128, 212
Mezger P. G., Mathis J. S., Panagia N., 1982, A&A, 105, 372
Miller J. H., Kelly H. P., 1972, Phys. Rev. A, 5, 516
Omont A., 1986, A&A, 164, 159
Purcell E. M., 1979, ApJ, 231, 404
Ragot B. R., 2002, ApJ, 568, 232
Readhead A. C. S. et al., 2004, ApJ, 609, 498
Rouan D., Léger A., Omont A., Giard M., 1992, A&A, 253, 498
Sutherland R. S., 1998, MNRAS, 300, 321
Thomas M. A., Humbertson J. W., 1972, J. Phys B, 5, L229
Watson R. A., Rebolo R., Rubiño-Martín J. A., Hildebrandt S., Gutiérrez C. M., Fernández-Cerezo S., Hoyland R. J., Battistelli E. S., 2005, ApJ, 624, L89
Weingartner J. C., Draine B. T., 2001a, ApJ, 548, 296
Weingartner J. C., Draine B. T., 2001b, ApJ, 134, 263

APPENDIX A: PLASMA DRAG : NUMERICAL CALCULATION OF $\mathcal{I}$ IN THE GENERAL CASE

The numerical calculation of $\mathcal{I}$ is tricky because it involves integrating an oscillating function which frequency goes to infinity at one limit of the integral, as $t(\alpha \to \alpha_e) \to \infty$. Here, we describe our implementation for both the positive and negative grain charges.

A1 Positively charged grains: $Z_g > 0$

We first make the change of variable

$$z = \sqrt{\gamma} \cot \frac{\alpha}{2}, \tag{A1}$$

where $\gamma = (e-1)/(e+1)$. The expression for the time is now

$$\omega t(z) = \frac{\omega b}{v} \frac{1}{\sqrt{e^2-1}} \left(\ln \frac{z+1}{z-1} + 2e \frac{z}{z^2-1} \right). \tag{A2}$$

The $\mathcal{I}$-integral is then

$$\mathcal{I} = 4\gamma \left[\Re \int_1^\infty e^{i\omega t(z)} \frac{z^2-\gamma}{(z^2+\gamma)^2} dz \right]^2 + 16\gamma^2 \left[\Im \int_1^\infty e^{i\omega t(z)} \frac{z}{(z^2+\gamma)^2} dz \right]^2. \tag{A3}$$

The functions inside the integrals are analytical on the complex plane, deprived from the branch cut $[-1, 1]$ on the real axis and the two poles $\pm i\sqrt{\gamma}$. The integrands are at least $\mathcal{O}(z^{-2})$ as $|z| \to \infty$. Moreover, for $y \to 0^+$,

$$\Re\left[i\omega t(1-iy)\right] \propto \Re\left[i \ln\left(-1 + \frac{2i}{y}\right) - \frac{e}{y} \right] < 0. \tag{A4}$$

Thus, using the fact that the integral over the lower right part of the complex plane vanish, we can replace our integrals by integrals over the axis

$$z = 1 - iy, \quad 0 < y < +\infty. \tag{A5}$$

Note that for $e \to 1$, $\mathcal{I} = \mathcal{O}(e-1)$, as one may expect from almost parabolic trajectories if the grain repels the ion. Also, in the limit $\omega b/v \to 0$, $\mathcal{I} \to (e^2-1)/e^2$.

A2 Negatively charged grains: $Z_g < 0$

This time we make the change of variable

$$z = \frac{1}{\sqrt{\gamma}} \tan \frac{\alpha}{2}. \tag{A6}$$

The expression for the time is now

$$\omega t(z) = \frac{\omega b}{v} \frac{1}{\sqrt{e^2-1}} \left(\ln \frac{z+1}{z-1} - 2e \frac{z}{z^2-1} \right). \tag{A7}$$

And we have

$$\mathcal{I} = 4\gamma \left[\Re \int_1^\infty e^{i\omega t(z)} \frac{1-\gamma z^2}{(1+\gamma z^2)^2} dz \right]^2 + 16\gamma^2 \left[\Im \int_1^\infty e^{i\omega t(z)} \frac{z}{(1+\gamma z^2)^2} dz \right]^2. \tag{A8}$$

The functions inside the integrals are analytical on the complex plane, deprived from the branch cut $[-1, 1]$ on the real axis and the two poles $\pm i/\sqrt{\gamma}$. This time $\Re(i\,\omega\,t)$ is negative for z close to 1 when $\Im z > 0$. Moreover, the two poles tend to infinity when $e \to 1$; so to avoid integrating too close to the poles, we integrate over the line

$$z = 1 + e^{i\pi/4} y, \quad 0 < y < +\infty. \tag{A9}$$

In that case, the integrals are not simply bounded anymore for nearly parabolic trajectories. One can show, by making the previous change of variables, that

$$\mathcal{I}\left(\frac{\omega b}{v}, e, Z_g < 0\right) = \exp \frac{2\pi\omega b}{v\sqrt{e^2-1}} \mathcal{I}\left(\frac{\omega b}{v}, e, Z_g > 0\right). \tag{A10}$$

This expression is ill behaved for nearly parabolic trajectories, as the exponential factor diverges whereas the $\mathcal{I}$-integral vanishes. In order to avoid numerical problems, in the case of nearly parabolic trajectories, we make the change of variables

$$u = \left(\tan \frac{\alpha}{2}\right)^{-1}. \tag{A11}$$

The expression for the $\mathcal{I}$-integral is then, for $e - 1 \ll 1$:

$$\mathcal{I} \approx 4 \left\{ \int_0^{\sqrt{\frac{2}{e-1}}} \cos\left[\frac{\omega b}{v}(e-1)(u + \frac{u^3}{3}) \right] \frac{u^2-1}{(u^2+1)^2} du \right\}^2 + 16 \left\{ \int_0^{\sqrt{\frac{2}{e-1}}} \sin\left[\frac{\omega b}{v}(e-1)(u + \frac{u^3}{3}) \right] \frac{u}{(u^2+1)^2} du \right\}^2. \tag{A12}$$

Note that in terms of the true anomaly f, we have $u = -\tan f/2$ and the expression for the time can be found in Geyling & Westerman (1971) (equation 2.3.9).

Here, again we integrate along $u = e^{i\pi/6} y$, $0 < y < \infty$, which cancels the $\mathcal{O}(u^3)$ real part of the time and maximizes its positive imaginary part at infinity. Note that for very small eccentricities, this is mainly a function of $(\omega b/v)(e-1)$.

APPENDIX B: QUANTUM TREATMENT OF INFRARED EMISSION

In Section 7, we computed the net angular momentum loss due to infrared emission using classical electrodynamics. Here, we reconsider the effect with a quantum calculation. We assume a spherically symmetric grain for simplicity and neglect vibration–rotation interaction. We will recover the classical result in the limit $J \gg 1$, which is applicable to the dust grains considered in this paper.

The Hilbert space of the grain is characterized by the vibrational quantum numbers (generically denoted $\boldsymbol{v}$) and the three rotation quantum numbers J, K, M, where K is the projection of angular momentum on to the grain z-axis. The energy levels are given by

$$E_{J,K,M,\boldsymbol{v}} = E^0_{\boldsymbol{v}} + \frac{\hbar^2 J(J+1)}{2I}, \tag{B1}$$

where I is the grain moment of inertia and $E^0_{\boldsymbol{v}}$ is the vibrational energy. The rotational wave functions are

$$\Psi_{J,K,M}(\chi) = \sqrt{\frac{2J+1}{8\pi^2}} D^J_{K,M}(\chi), \tag{B2}$$

where $\chi = (\theta, \phi, \psi) \in \mathrm{SO}(3)$ is the set of Euler angles, $8\pi^2$ is the volume of SO(3) and $\mathbf{D}^J$ is the passive rotation matrix in the spin-J representation, i.e. $D^J_{M_1,M_2} = \langle J M_{1\,\mathrm{grain}} | J M_{2\,\mathrm{lab}} \rangle$.

Spontaneous infrared vibrational transitions are possible from vibrational state $\boldsymbol{v}'$ to $\boldsymbol{v}$, their rate is given by

$$A_{J,K,M,\boldsymbol{v}\to J',K',M',\boldsymbol{v}'} = \frac{4(E_{J,K,M,\boldsymbol{v}} - E_{J',K',M',\boldsymbol{v}'})^3}{3\hbar^4 c^3} \times |\langle J', K', M', \boldsymbol{v}'|\boldsymbol{\mu}|J., K, M, \boldsymbol{v}\rangle|^2, \tag{B3}$$

where $\boldsymbol{\mu}$ is the electric dipole moment operator. In the absence of vibration–rotation interaction, we may take the operator $\boldsymbol{\mu}$ to depend only on the vibrational quantum numbers and on the rotation matix $\mathbf{R}(\chi)$ that converts grain-fixed to lab-fixed coordinates:

$$\langle J', K', M', \boldsymbol{v}'|\boldsymbol{\mu}|J., K, M, \boldsymbol{v}\rangle = \langle J', K', M'|\mathbf{R}(\chi)|J., K, M\rangle \langle \boldsymbol{v}'|\boldsymbol{\mu}^{(g)}|\boldsymbol{v}\rangle. \tag{B4}$$

Here, $\boldsymbol{\mu}^{(g)}$ is the dipole moment in grain coordinates.

The transition rates can be determined by writing $\boldsymbol{\mu}^{(g)}$ in the polar basis,

$$\mu^{(g)}_0 = \mu^{(g)}_z \quad \text{and} \quad \mu^{(g)}_{\pm 1} = \frac{\mp\mu^{(g)}_x + \mathrm{i}\mu^{(g)}_y}{\sqrt{2}}, \tag{B5}$$

in which $\{\mu^{(g)}_m\}^1_{m=-1}$ transform in the $L = 1$ representation of SO(3). Written in this basis, the rotation matrix $\mathbf{R}(\chi)$ is the inverse of $\mathbf{D}^1(\chi)$, which for unitary $\mathbf{D}^1$ is the same as the Hermitian conjugate:

$$\langle J', K', M', \boldsymbol{v}'|\mu_m|J., K, M, \boldsymbol{v}\rangle = \langle J', K', M'|D^{1*}_{m',m}(\chi)|J., K, M\rangle \langle \boldsymbol{v}'|\mu^{(g)}_{m'}|\boldsymbol{v}\rangle. \tag{B6}$$

The first matrix element can be evaluated by the three rotation matrix integral,

$$\begin{aligned}
&\langle J', K', M'|D^{1*}_{m',m}(\chi)|J, K, M\rangle \\
&= \frac{\sqrt{(2J'+1)(2J+1)}}{8\pi^2} \\
&\times \int D^{J'*}_{K',M'}(\chi) D^{1*}_{m',m}(\chi) D^J_{K,M}(\chi)\, \mathrm{d}^3\chi \\
&= \sqrt{(2J'+1)(2J+1)}(-1)^{K'+m'+M'+m} \\
&\times \begin{pmatrix} J' & 1 & J \\ -K' & -m' & K \end{pmatrix} \\
&\times \begin{pmatrix} J' & 1 & J \\ -M' & -m & M \end{pmatrix}.
\end{aligned} \tag{B7}$$

This transforms the spontaneous decay rate (equation B3) into

$$\begin{aligned}
&\frac{4(E_{J,K,M,\boldsymbol{v}} - E_{J',K',M',\boldsymbol{v}'})^3}{3\hbar^4 c^3}(2J'+1)(2J+1) \\
&\times \sum_{m=-1}^{1} \left| \sum_{m'=-1}^{1} (-1)^{m'} \langle \boldsymbol{v}'|\mu^{(g)}_{m'}|\boldsymbol{v}\rangle \right. \\
&\times \begin{pmatrix} J' & 1 & J \\ -K' & -m' & K \end{pmatrix} \\
&\times \left. \begin{pmatrix} J' & 1 & J \\ -M' & -m & M \end{pmatrix} \right|^2.
\end{aligned} \tag{B8}$$

We would now like to find the net decay rates to states of different J'. To do this, we assume the grain is randomly oriented, i.e. we average over initial projections K and sum over final projections K'. Using the $3j$ symbol orthonormality relations, one obtains

$$\begin{aligned}
A_{J,M,\boldsymbol{v}\to J',M',\boldsymbol{v}'} &= \frac{4(E_{J,\boldsymbol{v}} - E_{J',\boldsymbol{v}'})^3}{3\hbar^4 c^3}(2J'+1) \\
&\times \sum_{m'} \left| \langle \boldsymbol{v}'|\mu^{(g)}_{m'}|\boldsymbol{v}\rangle \right|^2 \\
&\times \sum_{m} \begin{pmatrix} J' & 1 & J \\ -M' & -m & M \end{pmatrix}^2.
\end{aligned} \tag{B9}$$

(The terms mixing different values of m' are eliminated by orthogonality relations.) The summation over m of course has at most one term, with $m = \Delta M \equiv M' - M$.

We are interested in the net angular momentum loss, which is most easily obtained by taking an initial state with $M = J$. There are then six possible values of ΔJ and ΔM, constrained by selection rules (ΔJ, $\Delta M = -1$, 0, $+1$) and the restriction $\Delta M \le \Delta J$. The branching ratios are constrained by (i) the energy difference factors in equation (B9), (ii) the factor of $2J' + 1$ and (iii) the $3j$ symbol. We consider each.

The energy factors do not depend on ΔM. If we take natural frequency $\nu = (E^0_{\boldsymbol{v}} - E^0_{\boldsymbol{v}})/h$, then the energies differences are given by

$$E_{J,\boldsymbol{v}} - E_{J',\boldsymbol{v}'} = h\nu - \frac{\hbar^2}{2I}(2J + 1 + \Delta J)\Delta J. \tag{B10}$$

The classical grain rotation rate is $\omega = \hbar J/I$. In the limit of $J \gg 1$ and $\omega \ll \nu$, the energy difference is proportional to $1 - \omega\Delta J/2\pi\nu$, so the cube of the energy difference is proportional to $1 - 3\omega\Delta J/2\pi\nu$.

The square of the $3j$ symbol, multiplied by $2J' + 1$, can be directly evaluated for the six cases of interest. It is

$$\begin{aligned}
\frac{2J-1}{2J+1} &\quad \Delta J = -1, \quad \Delta M = -1, \\
\frac{1}{J+1} &\quad \Delta J = 0, \quad \Delta M = -1, \\
\frac{J}{J+1} &\quad \Delta J = 0, \quad \Delta M = 0, \\
\frac{1}{(J+1)(2J+1)} &\quad \Delta J = +1, \quad \Delta M = -1, \\
\frac{1}{J+1} &\quad \Delta J = +1, \quad \Delta M = 0 \text{ and} \\
1 &\quad \Delta J = +1, \quad \Delta M = +1.
\end{aligned} \tag{B11}$$

By multiplying these relative probabilities by $1 - 3\omega\Delta J/2\pi\nu$, it is easily seen that the average $\langle \Delta M \rangle$ is exactly zero if $\omega = 0$. Therefore, the leading contribution to $\langle \Delta M \rangle$ can be obtained by taking the large-J limit of the $3j$ symbols. Transitions with $\Delta J \neq \Delta M$

are suppressed by powers of J in equation (B11), so one has three available transitions: $\Delta M = -1, 0, +1$, $\Delta J = \Delta M$. Since the factors in equation (B11) go to unity, the branching ratio for these three transitions is determined entirely by the energy factor

$$P(\Delta M) = \frac{1}{3} - \frac{\omega}{2\pi\nu}\Delta M. \tag{B12}$$

This implies an average loss of z-component of angular momentum

$$\langle \Delta M \rangle = -\frac{\omega}{\pi\nu}. \tag{B13}$$

In particular, we may find the ratio of angular momentum loss to energy loss ($h\nu$), which is

$$\frac{\dot{L}_z}{\dot{E}} = \frac{\hbar\omega/\pi\nu}{h\nu} = \frac{\omega}{2\pi^2\nu^2}. \tag{B14}$$

With the normalization of equation (150) and this ratio, one recovers equation (151).

This paper has been typeset from a TEX/LATEX file prepared by the author.